

# Single-platelet nanomechanics measured by high-throughput cytometry

---

ML Smith, DR Myers, Y Qiu, ME Fay, M Tennenbaum, D Chester, J Cuadrado, Y Sakurai, J Baek, R Tran, J Ciciliano, B Ahn, R Mannino, S Bunting, C Bennett, M Briones, A Fernandez-Nieves, AC Brown, T Sulchek, WA Lam. "Single-platelet nanomechanics measured by high-throughput cytometry." *Nature Materials*,

<https://hdl.handle.net/2144/18019>

*"Downloaded from OpenBU. Boston University's institutional repository."*

1 Resolving the nanomechanics of platelet contraction, the driver of blood clot stiffening, towards  
2 clinical translation

3 David R. Myers<sup>1,2,3,4,5</sup>, Yongzhi Qiu<sup>1,2,3,4,5</sup>, Meredith E. Fay<sup>1,2,3,4,5</sup>, Michael Tennenbaum<sup>6</sup>,  
4 Daniel Chester<sup>7,8</sup>, Jonas Cuadrado<sup>6</sup>, Yumiko Sakurai<sup>1,2,3,4,5</sup>, Jong Baek<sup>1,2,3,4,5</sup>,  
5 Reginald Tran<sup>1,2,3,4,5</sup>, Jordan Ciciliano<sup>1,2,3,4,5</sup>, Byungwook Ahn<sup>1,2,3,4,5</sup>, Robert Mannino<sup>1,2,3,4,5</sup>,  
6 Silvia Bunting<sup>9</sup>, Carolyn Bennett<sup>1</sup>, Michael Briones<sup>1</sup>, Alberto Fernandez-Nieves<sup>6</sup>,  
7 Michael L. Smith<sup>10</sup>, Ashley Carson Brown<sup>7,8</sup>, Todd Sulchek<sup>11</sup>, Wilbur A. Lam<sup>1,2,3,4,5</sup>

8

9

10 <sup>1</sup> Department of Pediatrics, Division of Pediatric Hematology/Oncology, Aflac Cancer Center and Blood Disorders Service of  
11 Children's Healthcare of Atlanta, Emory University School of Medicine, Atlanta, GA 30322

12 <sup>2</sup> The Wallace H. Coulter Department of Biomedical Engineering, Georgia Institute of Technology & Emory University, Atlanta,  
13 GA, 30332

14 <sup>3</sup> Winship Cancer Institute of Emory University, Atlanta, GA, 30322

15 <sup>4</sup> Parker H. Petit Institute of Bioengineering and Bioscience, Georgia Institute of Technology, Atlanta, GA 30332

16 <sup>5</sup> Institute for Electronics and Nanotechnology, Georgia Institute of Technology, Atlanta, GA 30332

17 <sup>6</sup> School of Physics, Georgia Institute of Technology, Atlanta, GA, 30332

18 <sup>7</sup> Department of Biomedical Engineering, North Carolina State University and  
19 University of North Carolina Chapel Hill, Raleigh, NC 27695

20 <sup>8</sup> Comparative Medicine Institute at North Carolina State University, Raleigh, NC 27695

21 <sup>9</sup> Department of Pathology, Emory University School of Medicine, Atlanta, GA 30322

22 <sup>10</sup> Department of Biomedical Engineering, Boston University, Boston, MA, 02215

23 <sup>11</sup> George W. Woodruff School of Mechanical Engineering, Georgia Institute of Technology, Atlanta, GA, 30332

24

25 Corresponding Author:

26 Wilbur A. Lam

27 Address: 2015 Uppergate Dr, NE; Emory Children's Center - Room 448; Atlanta, GA 30322

28 Email: [wilbur.lam@emory.edu](mailto:wilbur.lam@emory.edu)

29 Phone: 404-727-7473

30 Fax: 404-727-4455

31 **Hemostasis occurs at sites of vascular injury where flowing blood forms a clot, a **dynamic****  
32 **and heterogenous fibrin-based biomaterial. Paramount in the clot's capability to stem**  
33 **hemorrhage are its **changing** mechanical properties, the major driver of which are the**  
34 **contractile forces exerted by platelets against the fibrin scaffold<sup>1</sup>. However, how platelets**  
35 **transduce microenvironmental cues to mediate contraction and alter clot mechanics is**  
36 **unknown yet clinically relevant, as overly softened and stiffened clots are associated with**  
37 **bleeding<sup>2</sup> and thrombotic disorders<sup>3</sup>, respectively. To that end, we developed a high-**  
38 **throughput platelet contraction cytometer to quantify single platelet contraction forces in**  
39 **different clot microenvironments and found that platelets, via the Rho/ROCK pathway,**  
40 **synergistically couple mechanical and biochemical inputs to mediate contraction.**  
41 **Moreover, highly contractile platelet subpopulations present in healthy controls are**  
42 **conspicuously absent in a subset of patients with undiagnosed bleeding diatheses and**  
43 **therefore may function as a clinical diagnostic biophysical biomarker.**

44 During clot formation, various physiological cues such as damaged blood vessels or shear forces  
45 initiate platelet activation, adhesion, and the coagulation cascade, which lead to fibrin  
46 polymerization. Activated platelets then aggregate and bind to the nascent fibrin network via the  
47  $\alpha_{IIb}\beta_3$  integrin and undergo actomyosin-mediated muscle-like contraction (Extended Data Figure  
48 1, Extended Data Video 1), which significantly decreases the overall clot size while increasing  
49 clot stiffness by several orders of magnitude. While this platelet-driven clot contraction has been  
50 well described in the literature, the mechanistic underpinnings and especially the biochemical  
51 and biophysical parameters that mediate this process remain poorly understood due to  
52 technological barriers. Current assays provide force measurements during clot contraction,

53 establishing changes in average platelet force with different diseases<sup>4</sup>, but these operate at the  
54 bulk level<sup>1,3,5,6</sup>.

55 As recent studies demonstrate, microenvironmental cues such as mechanical properties of the  
56 underlying matrix substrate<sup>7,8</sup>, matrix geometry<sup>9</sup>, biochemical conditions<sup>10</sup>, and shear stress  
57<sup>11,12</sup> all mediate platelet physiology at the single cell level. In addition, clots in the dynamic  
58 hemodynamic environment are innately heterogeneous in which shear rate, fibrin architecture,  
59 and agonist concentration all vary significantly throughout the same clot. Therefore, a high-  
60 throughput, single platelet contraction assay is needed to establish and understand the  
61 “fundamental driver” of clot contraction, that is, how an individual platelet integrates  
62 biochemical and biophysical inputs to contract against the microenvironmental fibrin/ogen  
63 network. As fibrin mechanics have been well characterized,<sup>13</sup> deciphering this fundamental  
64 driver of clot contraction is the “missing link” needed to reconstruct higher order clot behavior  
65 and to obtain a comprehensive physical understanding of clot mechanics at multiple length  
66 scales.

67 To that end, we developed a microfabricated chip that simultaneously measures the contractile  
68 force of hundreds of individual platelets adherent on substrates with varied mechanical  
69 stiffnesses spanning the physiological range, while controlling the biochemical and shear  
70 microenvironment. This system overcomes technical barriers associated with existing techniques  
71 used for single cell analysis, such as the low throughput of atomic force microscopy<sup>8</sup>; the high  
72 computational needs of traction force microscopy<sup>14</sup>; or aggregate platelet measurements with  
73 micropillar arrays<sup>15</sup>. Here, an activated platelet adheres to and spans a fibrinogen microdot pair  
74 and contracts the microdot pair together (Figure 1a-c, Extended Data Video 4). As contraction  
75 force is proportional to the fibrinogen microdot area and microdot displacement, relatively high-

76 throughput measurements conducted with single cell resolution (Figure 1d-e), effectively  
77 creating a “platelet contraction cytometer.” Imaging studies of the fibrin architecture in a  
78 developing clot informed microdot spacing/size (Extended Data Figure 1, Supplementary  
79 Information, and Methods: Optimizing plating), recapitulating the geometry of the *in vivo*  
80 platelet microenvironment. **Since the platelet behavior of spanning and pulling microdots  
81 together is morphologically similar to clot behavior of platelets in fibrin meshes, trends observed  
82 in this system are expected to match those observed in a 3D system.** Hydrogel stiffnesses of 5 –  
83 100 kPa were used to approximate the range of mechanical environments encountered by a  
84 platelet within a clot (Extended Data Figure 2).

85 Because local biochemical agonists, hemodynamics, and mechanical properties of the clot  
86 directly mediate platelet physiology, we further refined our microfluidic system to enable  
87 encapsulation of micropatterned hydrogels of different stiffnesses in adjacent microchannels,  
88 enabling simultaneous testing of substrate stiffnesses, shear conditions, or agonist concentrations  
89 (Figure 2a-b, Extended Data Figure 3). **Each measurement of contraction force is not influenced  
90 by confounding effects such as the underlying substrate or neighboring platelet contraction, as  
91 shown by measurements of the gel thickness, stiffness, and microdot independence (Extended  
92 Data Figure 4).** As thrombin, a potent physiologic platelet activator, and substrate stiffness both  
93 mediate different signaling pathways<sup>7</sup> that converge in clot contraction<sup>16</sup>, the contraction  
94 cytometer was used to quantify how platelets synergistically integrate both biochemical and  
95 microenvironmental mechanical inputs to modulate contractile forces. **Thrombin also converts  
96 fibrinogen to monomeric fibrin, enabling the experiments to more closely resemble the *in vivo*  
97 clotting environment<sup>17,18</sup>.**

98 Platelets have a highly nonlinear force curve (Figure 3) with maximum “peak” contraction force  
99 at moderate substrate stiffness and thrombin concentration, both within the physiologic range  
100 found in clots. While the observation of a peak force is similar to myocytes<sup>19</sup>, platelets are  
101 unique in that output force is both mediated and requires a biochemical and mechanical input.  
102 Surprisingly, platelet contraction force is independent of shear stress (Extended Data Figure 5).  
103 As measurements are obtained after initial adhesion **in our protocol**, this independence suggests  
104 that shear effects are most significant in the early phases of activation. Interestingly, at the  
105 highest tested thrombin concentrations (**5U/mL**) characteristic of prothrombotic conditions, the  
106 subset of low contractile force platelets increases, thereby lowering the average platelet force  
107 (**Figure 3**). In addition, at highest stiffness conditions, platelets contract at lower forces  
108 demonstrating that this phenomenon is not simply due to the sensitivity limit of our system  
109 (Extended Data Figure 6).

110 Mechanistically, we discovered that the substrate stiffness-mediated platelet contractile force is  
111 highly dependent on the Rho/ROCK pathway (Figure 4a). To elucidate the underlying  
112 mechanotransductive mechanisms of how clot stiffness mediates contraction force, we employed  
113 two pharmacologic inhibitors of myosin light chain phosphorylation, ML7 and Y276232, which  
114 inhibit Ca<sup>2+</sup>/calmodulin-dependent myosin light chain kinase (MLCK) and Rho kinase (ROCK),  
115 respectively. In light of previous results showing that MLCK and not ROCK is essential to  
116 mechanosensitive spreading<sup>7</sup>, our results showing ROCK and not MLCK is essential to  
117 mechanosensitive contraction highlight that the MLCK and ROCK pathways serve  
118 complementary mechanosensing functions in platelets. Previous studies have shown that the  
119 Rho/ROCK pathway is upregulated in cells adhered onto stiff environments<sup>20</sup> (RhoA) and is  
120 associated with stress fiber formation<sup>21</sup> (ROCK). Consistent with this idea is the observation

121 that actin polymerization weakly correlates with increasing platelet contractile force (Extended  
122 Data Figure 7). As the platelet is anucleate, our data also demonstrate that mechanosensitive  
123 contraction can occur in the absence of gene expression.

124 To determine whether these findings on single platelets are related to changes in the bulk  
125 material properties of a blood clot, we conducted ROCK-inhibition experiments using standard  
126 bulk clot contraction assays and bulk clot rheometry. We observed that ROCK-inhibition impairs  
127 bulk clot contraction as compared to the untreated control clots (Figure 4b), whereas MLCK  
128 inhibition did not alter clot contraction (Figure 4c). Bulk clot rheometry experiments, which  
129 enabled simultaneous measurements of storage and loss moduli as well as bulk tensile forces,  
130 revealed that while both control and ROCK-inhibited clots undergo a dramatic stiffening process  
131 during the course of the experiment (Figure 4d), the exerted tensile forces differed but only at  
132 later time points. Specifically, control and ROCK-inhibited clots apply similar forces during the  
133 beginning of clot formation (Figure 4e) when the measured storage and loss moduli are low  
134 (Figure 4d). Over time, as the clots stiffen (Figure 4d), ROCK-inhibited bulk clots begin to exert  
135 lower tensile forces (Figure 4e) and plateau while the control continues to increase over time.  
136 Taken together, these bulk clot contraction observations are consistent with our data on  
137 individual platelet contractile force. In soft environments, both ROCK-inhibited individual  
138 platelet forces and ROCK-inhibited bulk contraction forces are similar to matching controls in  
139 bulk and at the single platelet level. In stiff environments, however, both ROCK-inhibited  
140 individual platelet forces and ROCK-inhibited bulk contraction and forces are substantially  
141 lower than matching controls. As changes in bulk contraction can be due to multiple reasons,  
142 including changes in fibrin or rates of platelet contraction, our ROCK-inhibition single platelet  
143 contraction data coupled with the bulk data, taken together, suggest that platelet contractile force

144 alone can mediate these changes in bulk material behavior of clots. Hence, our data on  
145 individual platelet behavior in varying microenvironments is not only associated with bulk clot  
146 contraction but can even inform the mechanisms occurring in bulk. Interestingly, the storage and  
147 loss modulus are the same for both ROCK-inhibited and control (Figure 4d), which may be due  
148 to the fact that the storage modulus of a clot is a function of both the density of cross-linking  
149 points<sup>22</sup>, as well as tensioning of loose fibrin fibers<sup>23</sup>.

150 Since *in vitro* clot contraction impairment is associated with limiting the maximum force exerted  
151 by a platelet, we hypothesized that low contractile forces measured at the single platelet level are  
152 associated clinical bleeding disorders. To that end, we first measured the platelets from patients  
153 with impaired cytoskeletal machinery, which were expected to have lower contractile forces.  
154 Compared to healthy controls, patients with defective actomyosin machinery such as those with  
155 Wiskott Aldrich (WAS) syndrome, which involve mutations of the actin-related WAS protein  
156 gene, or MYH9-related disorders (MYH9RD), which involve mutations of the non-muscle  
157 myosin IIA gene, lack highly contractile platelets. Blood from WAS and MYH9 patients exhibit  
158 impaired bulk clot retraction,<sup>24,25</sup> but these studies could not definitively pinpoint specific  
159 dysfunction in platelet contraction<sup>25</sup>. In our system, platelets from these patients exhibited  
160 significantly lower contraction force compared to those from healthy individuals in both stiff  
161 (Figure 5a) and soft mechanical environments (Extended Data Figure 8). More specifically, in  
162 these patients, a larger platelet subpopulation exerts near zero contractile force on stiff  
163 environments than for healthy subjects - approximately 30% versus 6% of platelets. Our single  
164 platelet measurements suggest that in these disorders, the impaired clot retraction may be due to  
165 the inability of individual platelets to apply appropriate forces.

166 Diminished platelet contractile forces were also found in a subset of a small cohort of patients  
167 presenting with chronic bleeding symptoms but normal clinical hemostasis tests. Specifically,  
168 these individuals have either normal or low-normal laboratory values for complete blood count,  
169 coagulation screening tests, platelet function (via PFA-100 or platelet aggregometry), or von  
170 Willebrand disease panels (Extended Data Table 1, [Extended Data Table 2](#)). Interestingly, three  
171 of the five patients showed impaired platelet contractility on stiff gels (Figure 5a), with a notable  
172 platelet subpopulation with forces below 20nN. Our platelet contraction cytometer's capability to  
173 detect these previous undiagnosable patients with bleeding diatheses, independent of existing  
174 clinical tests of hemostasis, establishes it as a potential new category of diagnostic to evaluate for  
175 platelet dysfunction.

176 As shown above, a key capability of platelet contraction cytometry is single cell resolution and  
177 the detection of different platelet subpopulations based on contractility, providing a more  
178 nuanced understanding of what influences clot stiffening. Currently used contraction assays  
179 measure only bulk platelet contractility and do not detect the low contractile subpopulation that  
180 potentially correlates with disease. Even amongst our healthy donors, average platelet contractile  
181 forces varied considerably. However, platelet contractility cytometry revealed subpopulations of  
182 highly contractile platelets (with peaks at 30 nN and higher), which is consistent amongst all  
183 healthy donors (Figure 5b). We also observed individuals both with highly variable and highly  
184 consistent platelet contraction at different points in time (Extended Data Figure 9), indicating  
185 that platelet contraction force might be affected by a number of different physiological  
186 conditions, but in aggregate, establish a range that is consistently higher than the subset of  
187 bleeding patients described above. Our test then represents an important step towards the goal of  
188 personalized medicine.

189 By precisely controlling the mechanical, chemical, and shear microenvironments, this work  
190 defines the fundamental driver of clot stiffening, thereby providing important, clinically relevant  
191 insights into clot mechanics. The platelet contractility cytometer presented herein entails a  
192 simple fabrication process and represents a key technological advance in rapid, high-throughput,  
193 single cell force analysis. Models linking microscale measurements to macroscale clot mechanics  
194 are now possible, where they were previously hindered by the inherent mechanical complexity of  
195 fibrin and the lack of data on how single platelets sense their microenvironment and apply force.  
196 **Our data shows for the first time that trends observed in individually contracting platelets are**  
197 **mirrored by changes in the bulk material properties of clots. Moreover, single platelet**  
198 **contraction measurements inform how the material properties of a nascent clot directly affect**  
199 **platelet contraction and vice-versa, a correlation not accomplished by bulk assays.** Our data  
200 further suggests that platelet contraction cytometry has the potential to serve as a useful addition  
201 to existing clinical tests of platelet function, as platelet contraction does not correlate with the  
202 currently used biomarkers of platelet activation (Extended Data Figure 7). Our newfound  
203 understanding of how platelet actuation directly affects clot formation and mechanics can be  
204 used to guide diagnostic strategies for thrombosis and bleeding disorders. Similarly, our  
205 contraction data and findings of the involved mechanotransductive pathways (Rho/ROCK)  
206 inform the development of pharmacological agents aimed at optimizing clot stiffness. Finally,  
207 this reductionist assay could be used to provide insight into other physiologically common cell  
208 and fibrous matrix systems that are often used in tissue engineering<sup>26</sup>.

209

210

## 211 **Methods:**

### 212 **Device design: Fabrication**

213 The device relies on the use of commercially available materials such as thin rolls of PDMS and  
214 rapid fabrication techniques such as laser cutting to achieve fabrication times of less than 8 hours  
215 per batch of devices (Extended Data Figure 3).

### 216 **Laser cut gel mold**

217 The first layer of the device will hold the polymerized patterned polyacrylamide gels and serve  
218 as the base layer. A laser cutter (Universal Laser Systems, VLS 3.5) is used to pattern long  
219 rectangular holes (1 mm x 25 mm) into a pre-fabricated sheet of PDMS (Rogers HT6240-0.01")  
220 (Extended Data Figure 3a). The PDMS sheets are ultrasonically cleaned with successive  
221 solutions of diluted Alconox, DI water, and ethanol. The sheets along with 24x40 mm No. 1  
222 coverslips (Fisher Scientific) are then treated with an O<sub>2</sub> plasma (Harrick Plasma, PDC-32G) and  
223 covalently bonded together. The bonding is greatly improved after an overnight heat treatment at  
224 60 C.

225 Once bonded together, the combined PDMS and coverslip piece was silanized. After an O<sub>2</sub>  
226 plasma treatment, pieces were incubated in a 10% (3-Aminopropyl)trimethoxysilane (Sigma  
227 281778) /90% Ethanol/ 0.01% Glacial acetic acid solution for 90 min at 60C. The pieces were  
228 then vigorously rinsed with 70%ETOH/30% DI water three times, then rinsed with DI water  
229 three times. To improve the PDMS flexibility and surface properties, the pieces were left in DI  
230 water for 1 hour at room temperature. The pieces were then incubated with a 2% glutaraldehyde

231 solution at room temperature for 30 minutes, then rinsed with DI water, and dried with  
232 compressed nitrogen.

### 233 **Ligand (fibrinogen) stamped coverslips and optimal concentration**

234 Stamped coverslips (No 1.5, 18mm x 18mm) were prepared using the lift-off method as  
235 described previously<sup>27</sup> (Extended Data Figure 3b). The silicon mold to create the fibrinogen  
236 microdots was etched using standard lithography and etching techniques to a depth of 800 nm.  
237 Fibrinogen conjugated to AlexaFluor 488, 594, or 647 (Thermo Fisher Scientific) was used  
238 depending on other selected fluorophores in the experiment. The fibrinogen was incubated  
239 on 10 mm x 10 mm x 3 mm PDMS squares at 30  $\mu\text{g}/\text{mL}$  for 1 hour, rinsed off, and dried with  
240 compressed nitrogen. The PDMS squares with incubated fibrinogen were then brought in contact  
241 with  $\text{O}_2$  treated silicon molds and removed to create a fibrinogen microdot pattern on the PDMS.  
242 The microdot pattern was then transferred onto an  $\text{O}_2$  plasma treated 18 mm x 18 mm coverslip.  
243 Previous work has demonstrated that platelet spreading is greatly affected by the ligand density<sup>28</sup>  
244 . Surprisingly, platelet spreading is enhanced on low ligand density surfaces as compared with  
245 high ligand density surfaces. We attempted to both lower and increase the ligand density on our  
246 gels approximately 10 fold by changing the concentration of fibrinogen incubated on the PDMS  
247 stamps. For cases of low fibrinogen concentration on polyacrylamide gels, platelet adhesion was  
248 greatly diminished on the patterned surface, precluding contraction measurements. In cases of  
249 high fibrinogen concentration, the micropattern shape was often greatly deformed and of  
250 inconsistent brightness upon hydrogel polymerization. As such, our tests focused on  
251 concentrations of 30  $\mu\text{g}/\text{mL}$ .

## 252 **Polyacrylamide gel casting**

253 To create wells for the polyacrylamide gel, the fibrinogen patterned coverslip was inverted and  
254 aligned over the hybrid 25 x 40 mm PDMS glass coverslip. This assembled piece was placed in  
255 an argon filled glovebox (MBraun UNILab plus) after observing a 30 minute incubation under  
256 vacuum in the glovebox antechamber. In the glovebox, and directly prior to use, pre-mixed  
257 polyacrylamide solutions with appropriate ratios of acrylamide to bis-acrylamide in PBS, were  
258 mixed with N,N,N',N'-Tetramethylethylenediamine (Sigma Aldrich, T9281), ammonium  
259 persulfate (Sigma Aldrich, A3678), and acrylic acid N-hydroxysuccinimide ester (Sigma,  
260 A8060)<sup>29</sup>. Using a 20  $\mu$ L pipette, gel solutions were cast into the wells and allowed to  
261 polymerize for 90 minutes. Ammonium persulfate concentrations and NHS concentrations were  
262 optimized for an argon atmosphere and are approximately 10x lower than previously published  
263 values<sup>29</sup>. The concentrations used typically create a thin, unpolymerized region near the PDMS  
264 walls, ensuring that the hydrogel is mechanically isolated from the PDMS well. After  
265 polymerization, gels were removed from the glovebox and the 18 mm x 18 mm coverslip was  
266 removed and discarded. Gels were stored in PBS overnight and for up to seven days at 4°C.

## 267 **Device Characterization**

268 Fabrication of polyacrylamide gel-based systems have previously been shown to be highly  
269 controllable and repeatable<sup>30</sup> and previous experimental research<sup>31</sup> and subsequent mechanical  
270 models<sup>32</sup> determined that for polyacrylamide gels with thicknesses of  $>70 \mu\text{m}$ , the underlying  
271 glass substrate does not contribute to the locally measured stiffness. Here, the gels within our  
272 microdevice system are consistently  $>250 \mu\text{m}$  in thickness (Extended Data Figure 4a ),  
273 effectively preventing substrate effects from the underlying glass surface. We also performed

274 atomic force microscopy measurements to determine the stiffness of the gel constructs.  
275 Measurements were performed on polyacrylamide gels in laser cut microchannels using a  
276 colloidal cantilever (sQube, CP-PNPL-PS-A) with a stiffness of 0.08 N/m and 1.98  $\mu\text{m}$  diameter  
277 polystyrene sphere. Gel stiffnesses were in agreement with our calculated predicted values, and  
278 those reported by the literature<sup>33</sup> (Extended Data Figure 4b).

279 Testing was performed to confirm that the microdot pairs are indeed independent of one another  
280 and that a contracting platelet does not affect the mechanics of the neighboring microdot pair.  
281 With this system, the displacement field around the applied point force is expected decay over  
282 relatively short distances, as predicted by previous work<sup>34</sup>. Here, the microdot pairs are spaced  
283 far apart (8  $\mu\text{m}$  or greater) relative to the microdot pair displacement caused by platelet  
284 contraction, which is on the order of 1  $\mu\text{m}$  or less. At this distance, displacements induced by  
285 neighboring contracting platelets are expected to be negligible. To confirm this, we analyzed the  
286 microdot displacements of a single contracting platelet surrounded by empty microdot pairs in  
287 real time, and show that movement occurs only in the microdots to which the platelet is attached  
288 (Extended Data Figure 4c-d). Some negligible movement may occur below the limit of detection  
289 of 0.05  $\mu\text{m}$ , which was determined from measuring peak-to-peak movement in stationary  
290 microdots with no adherent platelets in the vicinity.

### 291 **PDMS microfluidic top**

292 PDMS microfluidics were cast from a SU-8 (Microchem Inc.) mold to create microfluidic  
293 channels and sized to cover the hydrogel strips. Microfluidics were 22 mm long x 1.5 mm wide,  
294 by 200  $\mu\text{m}$  tall. To assemble, the gels were rinsed with DI water and dried to the extent that all  
295 water on the coverslip-PDMS piece was removed. This is greatly facilitated by the fact that the

296 PDMS remains hydrophobic and the polyacrylamide gels are hydrophilic. The PDMS  
297 microfluidic was then quickly attached using a laser cut silicone adhesive (3M, 91022) to ensure  
298 that the gels do not dry during assembly. PBS was then flown into the enclosed channels until it  
299 was ready for use. The double sided tape approach is unique in that it provides rapid attachment  
300 of a microfluidic without affecting the patterned proteins.

### 301 **Coverslip hybrid microfluidic top**

302 The PDMS microfluidics were best suited to experiments requiring the use of shear flow. For  
303 experiments involving static flow conditions, a hybrid lid composed of laser cut PDMS and a  
304 coverslip facilitated imaging. Similar to conditions outlined above, premade PDMS sheets  
305 (Rogers HT6240-0.01”) were laser cut with well patterns, cleaned, and bonded to 18 mm x  
306 18 mm No 1. glass coverslips. Using the same procedure outline in the PDMS microfluidic top,  
307 the coverglass and PDMS hybrid lid is bonded to the hydrogel device layer using laser cut  
308 silicone adhesive. Upon experimental completion, the ends of the device may be sealed with  
309 silicone grease for multi-day storage.

## 310 **Experimental Methods**

### 311 **Platelet preparation**

312 Healthy blood donors and patient donors had abstained from aspirin in the last two weeks, and  
313 consent was obtained according to GT IRB H15258. Blood was drawn by median venipuncture  
314 into acid-citrate-dextrose (ACD) solution 2. The sample was subsequently centrifuged at 150 G  
315 for 15 min, and the resulting platelet rich plasma was gel filtered into HEPES modified Tyrodes  
316 buffer as described previously<sup>35</sup>. Platelets were diluted to a final concentration of  $4 \times 10^6/\text{mL}$  in  
317 Tyrodes buffer to minimize potential paracrine signaling. This equated to an average distance

318 between microdot pairs of 30-50 microns depending on the donor. In some experiments, platelets  
319 were incubated for 1 hour with vehicle (dimethyl sulfoxide, DMSO); ROCK inhibitor Y-27632  
320 at 50  $\mu\text{m}$  (Sigma Y0503), or MLCK inhibitor at 10  $\mu\text{m}$  (Sigma I2764).

321 For bulk contraction studies, blood was drawn by median antecubital venipuncture into acid-  
322 citrate-dextrose (ACD) solution 2. The sample was centrifuged 150 G for 15 min and the  
323 resulting platelet rich plasma was collected, and centrifuged with an additional 10% ACD by  
324 volume at 900G for 5min. The supernatant, platelet poor plasma, was discarded and the platelets  
325 were resuspended into HEPES modified Tyrodes buffer.

### 326 **Microdevice plating**

327 Immediately prior to loading platelets into the microfluidic the following was added: 5 mM of  
328  $\text{CaCl}_2$ , 5 mM of  $\text{MgCl}_2$ , 3  $\mu\text{g}/\text{mL}$  of fibrinogen, thrombin (Haematologic Technologies, Inc), and  
329 any relevant inhibitors. The small dimensions of the microfluidic ensure that platelets rapidly  
330 move to the ligand interaction region after activation. After 15 minutes, 60  $\mu\text{L}$  of a wash solution  
331 consisting of 5 mM of  $\text{CaCl}_2$ , 5 mM of  $\text{MgCl}_2$ , thrombin, and any relevant inhibitors was used to  
332 remove residual platelets from solution. Thrombin both activates the platelets and converts  
333 microdot fibrinogen into monomeric fibrin, more closely recapitulating the in vivo environment  
334 <sup>17,18</sup>. For some experiment involving shear stress, flow was applied using syringe pumps (PhD  
335 Ultra, Harvard Apparatus) with the wash solution to create a shear rates of either  $500\text{s}^{-1}$  or  $1000\text{s}^{-1}$ .  
336 The adhered platelets were then incubated for 90 minutes, which is several times more than  
337 needed for contraction to ensure that all platelets had sufficient time to reach a final state of  
338 contraction. Platelets were then fixed with a solution of Tyrodes buffer with 4%  
339 paraformaldehyde, 5 mM  $\text{CaCl}_2$ , and 5 mM  $\text{MgCl}_2$  for 15 minutes.

340 **Coverslip preparation & plating**

341 In conditions where a platelet sample was extremely rare (WAS, MYH9-RD), was imaged live,  
342 or required later mounting for high resolution imaging, micropatterned gels on 25 mm coverslips  
343 were used. Bottom coverslips were prepared by silanized using the method described above, and  
344 top coverslips were micropatterned using the technique described above. Gels were then  
345 prepared and placed in between the coverslips. Similar plating protocols were used, with the  
346 exception that gel coverslips were placed in 6 well plates, and platelet concentrations were  
347 dropped to 2M/mL.

348 **Plating optimization:**

349 Platelet behavior is affected by many different behaviors paracrine signaling, ligand density<sup>28</sup>,  
350 ligand type, and shear stress<sup>11</sup>. The device presented in this paper sought to quantify changes in  
351 platelet contraction due to differences in substrate stiffness and thrombin concentration, while  
352 holding all other parameters constant.

353 *ADP:* Our initial experiments examining the effect of ADP on platelet contraction were  
354 inconsistent for the same individuals and over time. Measured forces were much lower than  
355 thrombin, but were extremely varied in both platelet adhesion and forces.

356 *Platelet Concentration:* Platelet behavior may be affected by nearby activated platelets. To  
357 minimize potential confounding effects, the platelet concentration chosen is purposefully low to  
358 ensure an average distance between contracting platelets of approximately 30 to 50 microns.

359 There may be some enhancement of platelet contraction by neighboring platelets, but early tests

360 with and without apyrase found no change in contraction measurements from the presence of  
361 apyrase.

362 *Ligand Density:* It is possible that order of magnitude changes in ligand density could affect  
363 outside-in signaling, as shown earlier <sup>7,28</sup>. We sought to examine this phenomenon but were  
364 constrained by the range of ligand densities that can be achieved using this system. Here,  
365 30 µg/mL was optimal, creating well defined, repeatable patterns which supported platelet  
366 adhesion. When the stamping solution was 3 µg/mL, platelet adhesion was poor. At 300 µg/mL,  
367 the fibrinogen formed sheets which had the propensity to curl, lowering pattern fidelity. Overall,  
368 we expect trends presented here to be preserved on different ligand densities in light of previous  
369 reports <sup>7</sup> showing mechanosensitive trends are similar in low and high ligand density  
370 environments.

371 Shear Stress: Platelets were incubated for 15 minutes with thrombin concentrations of 0.1 or  
372 1 U/mL on the polyacrylamide gels to ensure adhesion. Shear rates of 500 and 1000 s<sup>-1</sup> applied  
373 for 1.5 hours to each thrombin concentration. Platelets were then fixed under flow with 4% PFA  
374 and imaged. No statistically significant differences were observed due to the application of shear  
375 stress from static controls at either thrombin concentration. Activating the platelets and allowing  
376 them to adhere to the fibrinogen under flow would enable shear stress to be applied during the  
377 entire activation process, leading to more firm conclusions that shear does not affect platelet  
378 contraction on fibrinogen with thrombin. Unfortunately, this condition is difficult to test as the  
379 constant flow of platelets also leads to multi-platelet aggregates.

## 380 **Immunocytochemistry**

381 After fixation, depending on the experiment, platelets were stained with an appropriate plasma  
382 membrane dye (Cell Mask Deep Red or Cell Mask Orange, Life Technologies). In some  
383 instances, platelets were counterstained with phalloidin (Alexa Fluor conjugated, Life  
384 Technologies) or phosphatidylserine with Annexin V (Alexa Fluor conjugated, Life  
385 Technologies). For detecting activated  $\alpha_{IIb}\beta_3$ , FITC-PAC-1 antibody (BD Biosciences) was  
386 applied to platelets after 75 minutes.

## 387 **Imaging & Mounting**

388 Gels were imaged on a Zeiss LSM 700-405 confocal microscope using a 20x 0.8 NA lens. For  
389 high resolution images, samples were rinsed with DI water, inverted and mounted onto  
390 coverslips (ProLong Gold Antifade, ThermoFisher Scientific). High resolution images of  
391 platelets were obtained using a GE Deltavision OMX Blaze using a 100x, 1.49 NA objective.

392 For high resolution scanning electron microscopy, samples were extracted from microfluidics,  
393 and incubated overnight in 50% ionic liquid (IL1000, Hitachi) and 50% deionized water. Excess  
394 liquid was wicked away using filter paper. Samples were imaged using a Hitachi SU8230 cold  
395 field emission SEM.

## 396 **Image Analysis**

397 Images were analyzed using a MATLAB script which measured the fibrinogen microdot areas,  
398 and calculated the center to center distance of the fibrinogen microdots. Due to the high pattern  
399 fidelity, the initial uncontracted distance was taken to be the distance of a neighboring pair of  
400 uncontracted microdots. Although minimized, occasional multi-platelet aggregates identifiable

401 by size occurred and were ignored. The current script and data collection is semi-automated,  
402 where confocal images are manually collected, and individual platelet pairs are identified by  
403 hand, then subsequently analyzed by the script. Such a system may readily be adapted for  
404 automation in future studies.

#### 405 **Bulk Isotonic Clot Contraction**

406 Polystyrene fluorimeter cuvettes (Sigma-Aldrich) with attached grids of 1 mm spacing were  
407 incubated with 1% F-127 pluronic (Sigma) at room temperature for 1 hour. A solution consisting  
408 of 2 mg/mL of purified human fibrinogen (FIB 3, Enzyme Research Laboratories), and  $250 \times 10^6$   
409 washed platelets/mL was prepared. This platelet-fibrin solution was then combined with 1U/mL  
410 of thrombin and 5mM CaCl<sub>2</sub> in the cuvette and kept at room temperature. Pictures of clot  
411 contraction were taken every 30 minutes, and clot volume was estimated using the attached grid.

#### 412 **Bulk Isometric Rheometry**

413 Rheological measurements were performed with a stress-controlled rheometer (Anton Paar MCR  
414 502) using cone-plate geometry. The clot was formed *in situ* and the shear moduli ( $G'$  and  $G''$ )  
415 as well as the normal force were measured as the clot forms. All measurements were done in the  
416 linear regime. Final clots composition consisted of: 2 mg/mL of purified human fibrinogen (FIB  
417 3, Enzyme Research Laboratories),  $250 \times 10^6$  washed platelets/mL, 1U/mL of thrombin, and 1  
418 mM CaCl<sub>2</sub>.

419

420

421 **References**

- 422 1. Jen, C. J. & McIntire, L. V. The structural properties and contractile force of a clot. *Cell*  
423 *Motil.* **2**, 445–55 (1982).
- 424 2. HVAS & Sørensen... Tranexamic acid combined with recombinant factor VIII increases  
425 clot resistance to accelerated fibrinolysis in severe hemophilia A. (2007). doi:10.1111/j.1538-  
426 7836.2007.02755.x
- 427 3. Collet, J. P. *et al.* Altered fibrin architecture is associated with hypofibrinolysis and  
428 premature coronary atherothrombosis. *Arterioscler. Thromb. Vasc. Biol.* **26**, 2567–73 (2006).
- 429 4. Carr, M. E. Development of platelet contractile force as a research and clinical measure  
430 of platelet function. *Cell Biochem. Biophys.* **38**, 55–78 (2003).
- 431 5. Cohen, I. & De Vries, A. Platelet contractile regulation in an isometric system. *Nature*  
432 **246**, 36–7 (1973).
- 433 6. Young, G. *et al.* Thrombin generation and whole blood viscoelastic assays in the  
434 management of hemophilia: current state of art and future perspectives. *Blood* **121**, 1944–1950  
435 (2013).
- 436 7. Qiu, Y. *et al.* Platelet mechanosensing of substrate stiffness during clot formation  
437 mediates adhesion, spreading, and activation. *Proc. Natl. Acad. Sci. U.S.A.* **111**, 14430–5 (2014).
- 438 8. Lam, W. A. *et al.* Mechanics and contraction dynamics of single platelets and  
439 implications for clot stiffening. *Nat Mater* **10**, 61–6 (2011).
- 440 9. Kita, A. *et al.* Microenvironmental geometry guides platelet adhesion and spreading: a  
441 quantitative analysis at the single cell level. *PLoS ONE* **6**, e26437 (2011).
- 442 10. Stalker, T. J. *et al.* Hierarchical organization in the hemostatic response and its  
443 relationship to the platelet-signaling network. *Blood* **121**, 1875–85 (2013).

- 444 11. Nesbitt, W. S. *et al.* A shear gradient-dependent platelet aggregation mechanism drives  
445 thrombus formation. *Nat. Med.* **15**, 665–73 (2009).
- 446 12. Kroll, M. H., Hellums, J. D., McIntire, L. V., Schafer, A. I. & Moake, J. L. Platelets and  
447 shear stress. *Blood* **88**, 1525–41 (1996).
- 448 13. Weisel, J. W. Biophysics. Enigmas of blood clot elasticity. *Science* **320**, 456–7 (2008).
- 449 14. Schwarz Henriques, S., Sandmann, R., Strate, A. & Köster, S. Force field evolution  
450 during human blood platelet activation. *Journal of cell science* **125**, 3914–20 (2012).
- 451 15. Liang, X. M., Han, S. J., Reems, J.-A. A., Gao, D. & Sniadecki, N. J. Platelet retraction  
452 force measurements using flexible post force sensors. *Lab Chip* **10**, 991–8 (2010).
- 453 16. Suzuki-Inoue, K. *et al.* Involvement of Src kinases and PLCgamma2 in clot retraction.  
454 *Thromb. Res.* **120**, 251–8 (2007).
- 455 17. Litvinov, RI, Gorkun, OV, Owen, SF & Shuman, H. Polymerization of fibrin:  
456 specificity, strength, and stability of knob-hole interactions studied at the single-molecule level.  
457 *Blood* (2005). at <<http://www.bloodjournal.org/content/106/9/2944.short>>
- 458 18. Litvinov, R. I. *et al.* Polymerization of fibrin: direct observation and quantification of  
459 individual B: b knob-hole interactions. *Blood* **109**, 130–138 (2007).
- 460 19. Engler, A. *et al.* Embryonic cardiomyocytes beat best on a matrix with heart-like  
461 elasticity: scar-like rigidity inhibits beating. *J Cell Sci* **121**, 3794–802 (2008).
- 462 20. Paszek, M. J. *et al.* Tensional homeostasis and the malignant phenotype. *Cancer Cell* **8**,  
463 241–54 (2005).
- 464 21. Burridge, K. & Wittchen, E. The tension mounts: Stress fibers as force-generating  
465 mechanotransducers. *The Journal of Cell Biology* **200**, 9–19 (2013).
- 466 22. De Gennes, P.-G. *Scaling Concepts in Polymer Physics*. (Cornell University Press).

- 467 23. Shah, J. & Janmey, P. Strain hardening of fibrin gels and plasma clots. *Rheol Acta* **36**,  
468 262–268 (1997).
- 469 24. Godwin, H. & Ginsburg, D. May–Hegglin Anomaly: A Defect in Megakaryocyte  
470 Fragmentation? *British Journal of Haematology* **26**, 117–127 (1974).
- 471 25. Shcherbina, A. *et al.* WASP plays a novel role in regulating platelet responses dependent  
472 on alphaIIb beta3 integrin outside-in signalling. *Br. J. Haematol.* **148**, 416–27 (2010).
- 473 26. Pedersen, J. A. & Swartz, M. A. Mechanobiology in the third dimension. *Ann Biomed*  
474 *Eng* **33**, 1469–90 (2005).
- 475 27. Von Philipsborn, A. C. *et al.* Microcontact printing of axon guidance molecules for  
476 generation of graded patterns. *Nat Protoc* **1**, 1322–8 (2006).
- 477 28. Jirousková, M., Jaiswal, J. K. & Coller, B. S. Ligand density dramatically affects integrin  
478 alpha IIb beta 3-mediated platelet signaling and spreading. *Blood* **109**, 5260–9 (2007).
- 479 29. Polio, S. R., Rothenberg, K. E., Stamenović, D. & Smith, M. L. A micropatterning and  
480 image processing approach to simplify measurement of cellular traction forces. *Acta Biomater* **8**,  
481 82–8 (2012).
- 482 30. Tse, J. R. & Engler, A. J. Stiffness gradients mimicking in vivo tissue variation regulate  
483 mesenchymal stem cell fate. *PLoS ONE* **6**, e15978 (2011).
- 484 31. Engler, A. J., Sen, S., Sweeney, H. L. & Discher, D. E. Matrix elasticity directs stem cell  
485 lineage specification. *Cell* **126**, 677–89 (2006).
- 486 32. Maloney, J. M., Walton, E. B., Bruce, C. M. & Van Vliet, K. J. Influence of finite  
487 thickness and stiffness on cellular adhesion-induced deformation of compliant substrata. *Phys*  
488 *Rev E Stat Nonlin Soft Matter Phys* **78**, 041923 (2008).

- 489 33. Tse, J. R. & Engler, A. J. Preparation of hydrogel substrates with tunable mechanical  
490 properties. *Curr Protoc Cell Biol* **Chapter 10**, Unit 10.16 (2010).
- 491 34. Sabass, B., Gardel, M., Waterman, C. & Schwarz, U. High Resolution Traction Force  
492 Microscopy Based on Experimental and Computational Advances. *Biophys J* **94**, 207–220  
493 (2008).
- 494 35. McCabe White, M. & Jennings, L. K. *Platelet Protocols: Research and Clinical*  
495 *Laboratory Procedures*. (Academic Press).
- 496 36. Gersh, K. C., Nagaswami, C. & Weisel, J. W. Fibrin network structure and clot  
497 mechanical properties are altered by incorporation of erythrocytes. *Thromb. Haemost.* **102**,  
498 1169–75 (2009).
- 499 37. Collet, J.-P. P., Shuman, H., Ledger, R. E., Lee, S. & Weisel, J. W. The elasticity of an  
500 individual fibrin fiber in a clot. *Proc. Natl. Acad. Sci. U.S.A.* **102**, 9133–7 (2005).
- 501
- 502

503 **End Notes:**

504

505 **Supplementary Information** is linked to the online version of the paper

506

507 **Acknowledgements:** The authors wish to thank Andrew Shaw of the Parker H. Petit Institute for  
508 Bioengineering and Bioscience at the Georgia Institute of Technology (GT); the Emory  
509 University Integrated Cellular Imaging Microscopy Core of the Children’s Pediatric Research  
510 Center; and the GT Institute for Electronics and Nanotechnology (IEN) cleanroom. Financial  
511 support provided by NIH R01 (HL121264) to WAL, an AHA Postdoctoral Fellowship to DRM.  
512 DRM thanks CRD and GAK for comments and discussion.

513

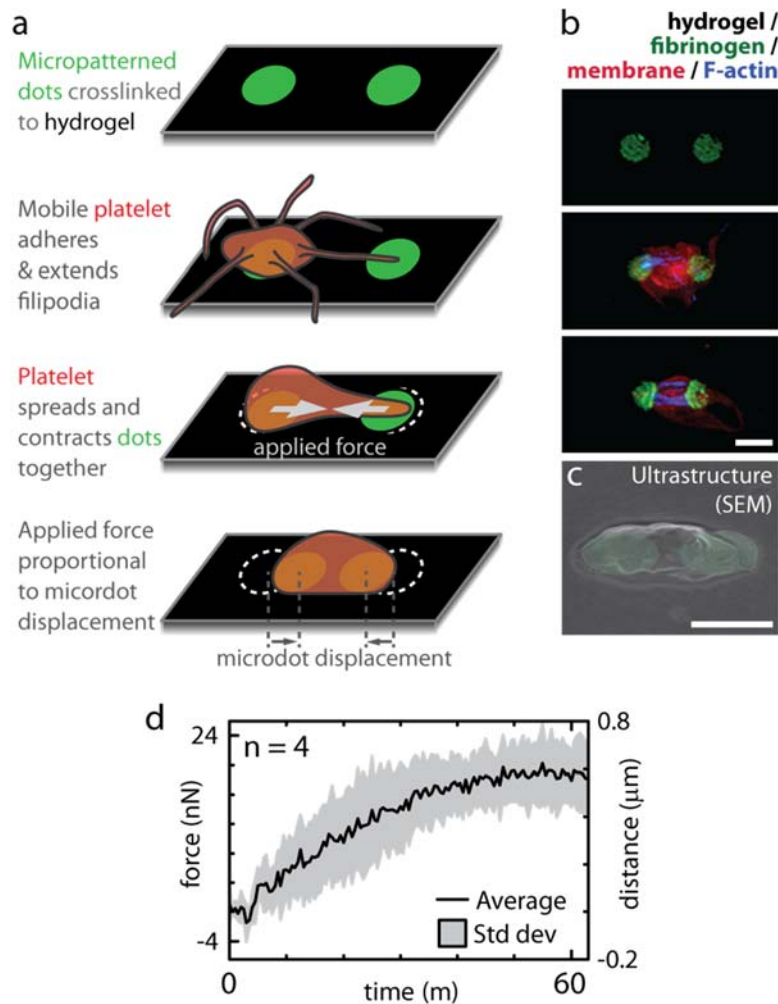
514 **Author Contributions:** DRM & WAL conceived of and designed platelet contraction  
515 experiments. DRM, YQ, ACB, JC, BA, MS, TS, & WAL designed and tested platelet  
516 contraction cytometer. DRM, YS, RT, RM, SB, CB, MB performed experiments. MEF designed  
517 and wrote image analysis algorithms. DRM & WAL analyzed data and wrote the manuscript.

518

519 **Author Information:** The authors declare no competing financial interests. Correspondence  
520 and requests for materials should be addressed to wilbur.lam@emory.edu

521

522



523

524 Figure 1: The fundamental unit driving clot stiffening, a single platelet pulling against a

525 fibrin/ogen substrate, is established by recapitulating the mechanical and biological

526 microenvironment of the platelet. **a**, Fluorescently-conjugated fibrinogen microdot pairs are

527 covalently bound to a deformable polyacrylamide hydrogel of known mechanical properties. As

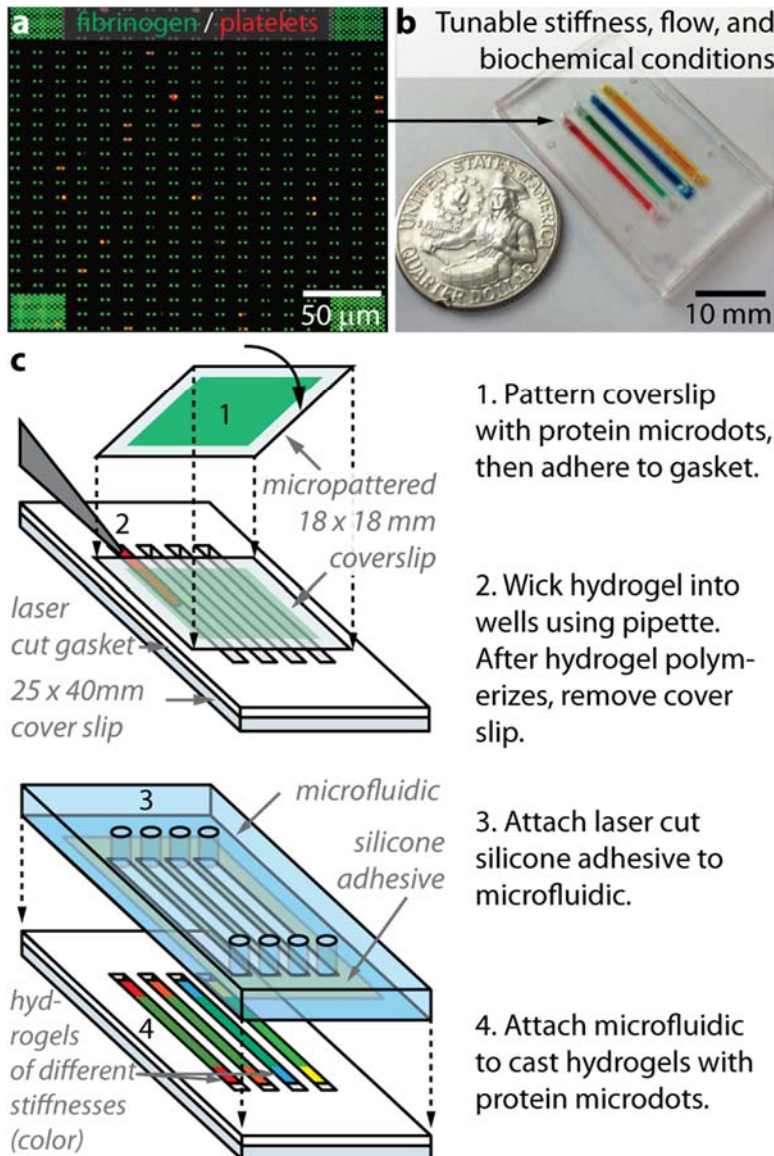
528 a platelet adheres and pulls pairs of fibrinogen microdots together, the contractile force is

529 proportional to the microdot displacement. **b**, Super-resolution microscopy images of individual

530 platelets with various degrees of contraction, scale bar is  $2\ \mu\text{m}$  **c**, Scanning electron microscopy

531 image of a platelet contracting a fibrinogen microdot pair, scale bar is  $2\ \mu\text{m}$ . **d**, Real time

532 contractile measurements of 4 single platelets.



533  
534 Figure 2: Platelet contraction cytometer - hydrogels with microprinted arrays of fibrinogen

535 microdots are encapsulated in separate microchannels, enabling the biochemical, mechanical,

536 and shear microenvironments to be precisely controlled and varied simultaneously. **a**, A confocal

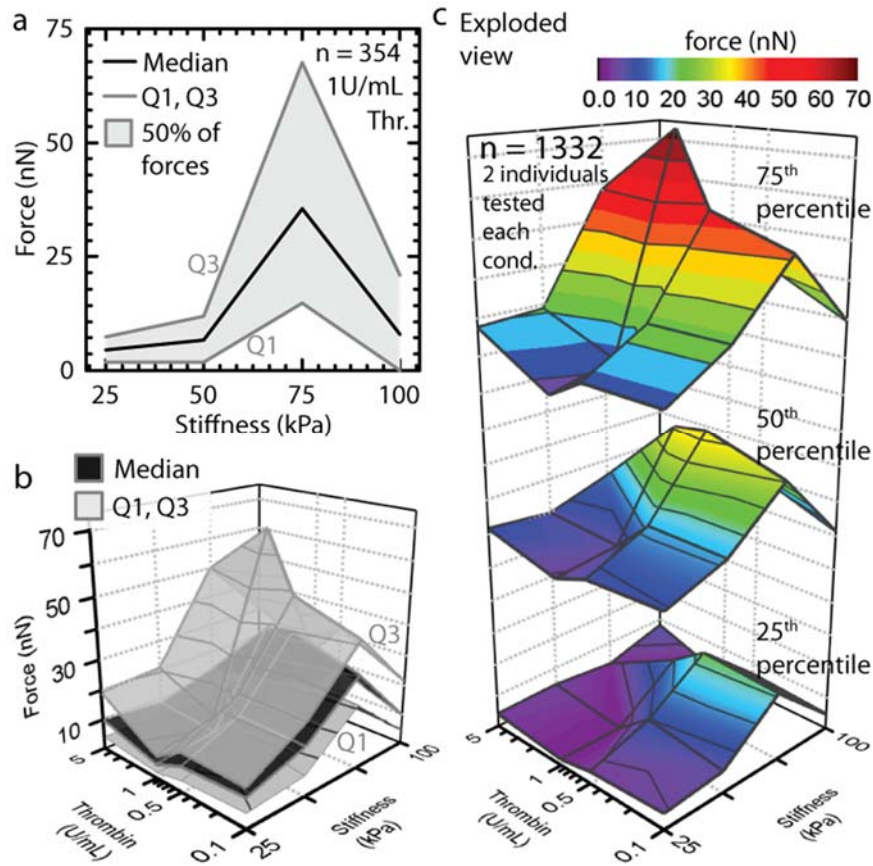
537 image showing single platelets (red, contracting against fibrinogen microdot pairs (green) on the

538 hydrogel surface. Over 20,000 fibrinogen microdot pairs are microprinted on the surface of each

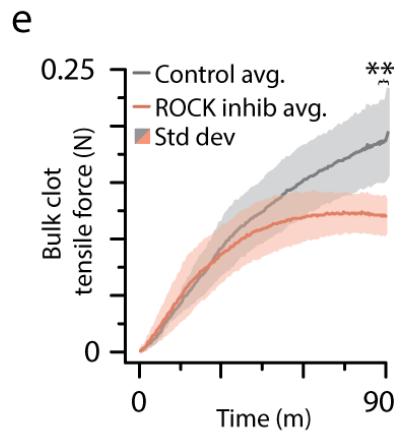
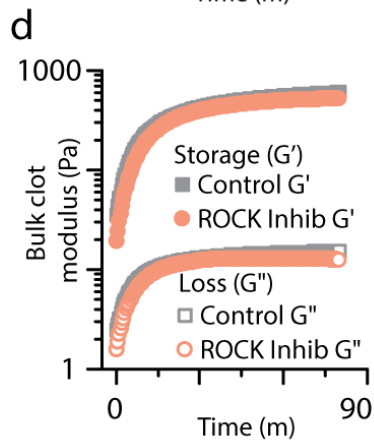
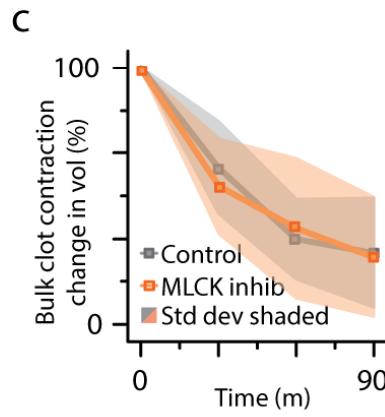
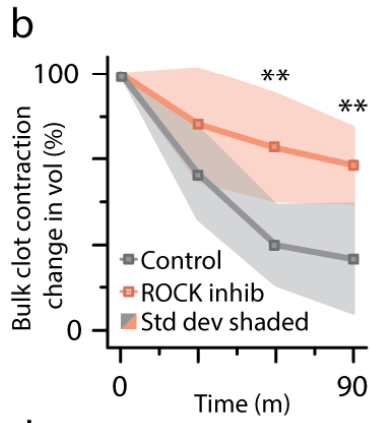
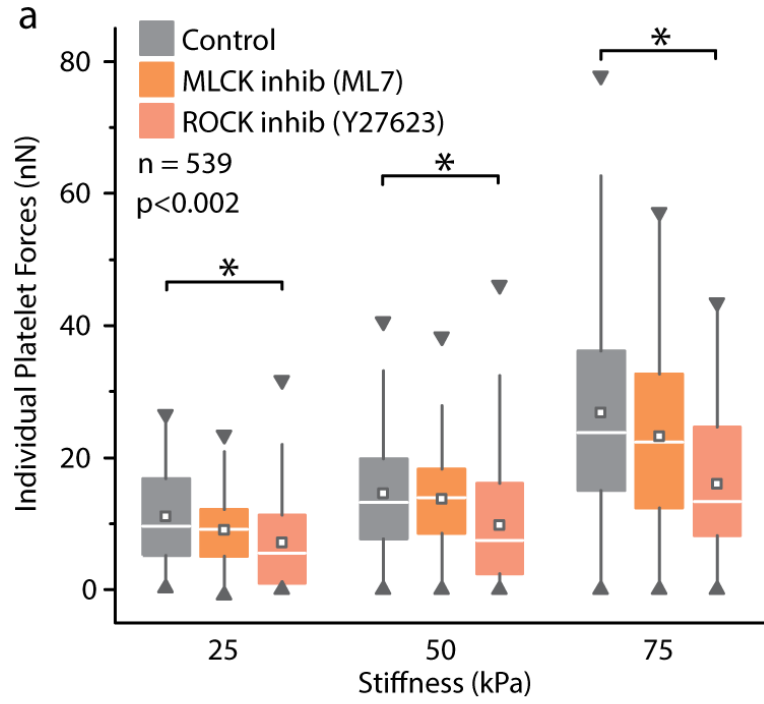
539 hydrogel encapsulated in each microchannel. **b**, Each microfluidic device may comprise different

540 variables,, here four of microchannels comprise of hydrogels of different stiffness. **c**, A novel yet

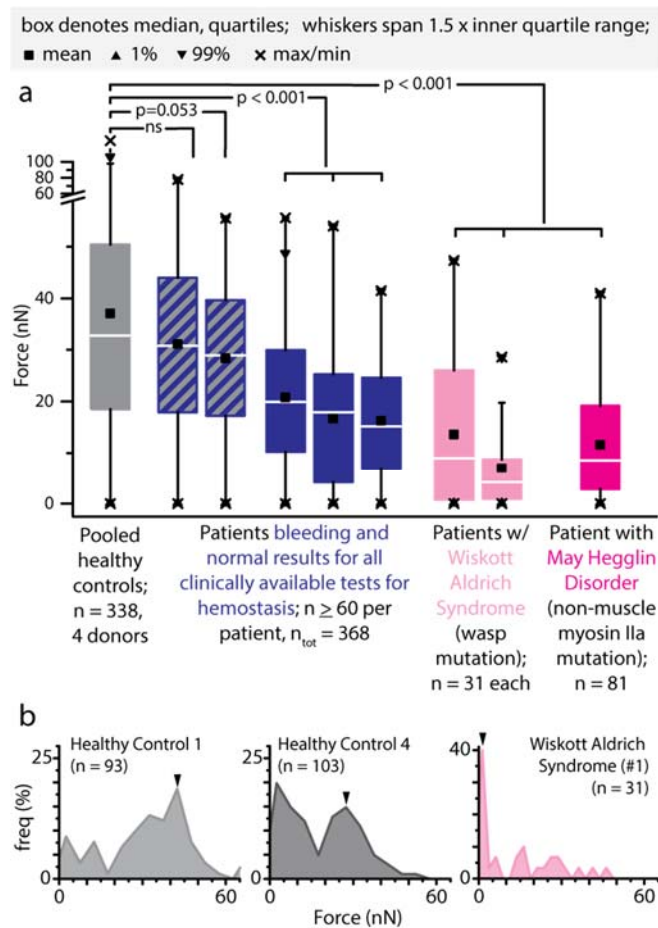
541 relatively simple fabrication process flow enables rapid manufacturing.



542  
 543 Figure 3: Biochemical and mechanical cues synergistically mediate platelet contraction force. **a**,  
 544 Maximal platelet contraction occurs at 75kpa substrate stiffness and 1U/mL thrombin. **b**, Single  
 545 platelet force quartiles for physiologically relevant clot stiffnesses and thrombin concentrations.  
 546 Platelet contractile forces are highest at a substrate stiffness of 75 kPa or at 5U/mL thrombin. A  
 547 minimum occurs at 25 kPa stiffness and 1U/mL thrombin. **c**, Exploded view of b to aid  
 548 visualization. Microenvironmental stiffness has a dominant role over thrombin concentration.  
 549 Force attenuation at the highest stiffness conditions suggests a mechanically mediated negative  
 550 feedback mechanism governing the upper limits of platelet contraction. n refers to total number  
 551 of platelets tested.



553 Figure 4: Mechanotransductive platelet contraction is mediated by the Rho-associated protein  
554 kinase (ROCK) pathway, as measured with platelet contraction cytometry and standard bulk clot  
555 contraction and bulk clot rheometry. **a**, The increase in platelet contractile forces with increasing  
556 substrate stiffness is significantly reduced with exposure to Y27623, a pharmacologic ROCK  
557 inhibitor. Pharmacologic inhibition of the myosin light chain kinase (MLCK) with ML7, on the  
558 other hand, did not produce a statistically significant difference in the substrate stiffness-  
559 mediated effect on platelet contractile force. Box denotes median and quartiles; whiskers to 1.5  
560 interquartile range), square denotes median, triangles denotes 1% and 99%. (n = 539, each  
561 condition n>40). \* indicates differences from control at same stiffness (p < 0.05 by Mann-  
562 Whitney). **b**, ROCK inhibition impairs bulk clot contraction (n = 4) as compared to the untreated  
563 control clots. **c**, MLCK inhibition does not change bulk clot contraction (n = 4). **d**, Oscillatory  
564 rheometry, which enables simultaneous measurements of storage and loss moduli as well as bulk  
565 tensile forces, revealed that both control and ROCK-inhibited clots undergo a dramatic stiffening  
566 process (representative plot from 3 similar experiments shown). The angular frequency and  
567 strain amplitude are 1 rad/s and 0.01, respectively, which are well within the linear regime of the  
568 samples. **e**, Control and ROCK-inhibited clots apply similar forces during the beginning of clot  
569 formation when the measured storage and loss moduli are low (n = 3). As the clots stiffen  
570 (Figure 4d), ROCK-inhibited bulk clots begin to exert lower tensile forces and plateau while the  
571 control continues to increase over time. \*\* indicates difference from control (p < 0.05 by t-test).



572  
 573 Figure 5: Patients with phenotypic bleeding lack highly contractile platelets associated with clot  
 574 contraction and force generation. **a**, Wiskott Aldrich Syndrome and May Hegglin Disorder  
 575 platelets exhibited significantly reduced contractile forces compared to that of healthy controls  
 576 (75 kPa gel stiffness, 1U/mL thrombin). In a subset of patients with bleeding diatheses yet  
 577 normal hemostasis tests, platelet contraction was lower than that of normal healthy controls.  
 578 **b**, Histogram data reveal platelet subpopulations of varying contractile forces. Healthy control  
 579 platelets comprise high contractility subpopulations, notably absent in platelets from a Wiskott  
 580 Aldrich Syndrome patient. In all panels, n refers to number of platelets, Mann-Whitney statistical  
 581 test.

582 **Figure Legends**

583 Figure 1: The fundamental unit driving clot stiffening, a single platelet pulling against a  
584 fibrin/ogen substrate, is established by recapitulating the mechanical and biological  
585 microenvironment of the platelet. **a**, Fluorescently-conjugated fibrinogen microdot pairs are  
586 covalently bound to a deformable polyacrylamide hydrogel of known mechanical properties. As  
587 a platelet adheres and pulls pairs of fibrinogen microdots together, the contractile force is  
588 proportional to the microdot displacement. **b**, Super-resolution microscopy images of individual  
589 platelets with various degrees of contraction, scale bar is 2  $\mu\text{m}$  **c**, Scanning electron microscopy  
590 image of a platelet contracting a fibrinogen microdot pair, scale bar is 2  $\mu\text{m}$ . **d**, Real time  
591 contractile measurements of 4 single platelets.

592 Figure 2: Platelet contraction cytometer - hydrogels with microprinted arrays of fibrinogen  
593 microdots are encapsulated in separate microchannels, enabling the biochemical, mechanical,  
594 and shear microenvironments to be precisely controlled and varied simultaneously. **a**, A confocal  
595 image showing single platelets (red, contracting against fibrinogen microdot pairs (green) on the  
596 hydrogel surface. Over 20,000 fibrinogen microdot pairs are microprinted on the surface of each  
597 hydrogel encapsulated in each microchannel. **b**, Each microfluidic device may comprise different  
598 variables,, here four of microchannels comprise of hydrogels of different stiffness. **c**, A novel yet  
599 relatively simple fabrication process flow enables rapid manufacturing.

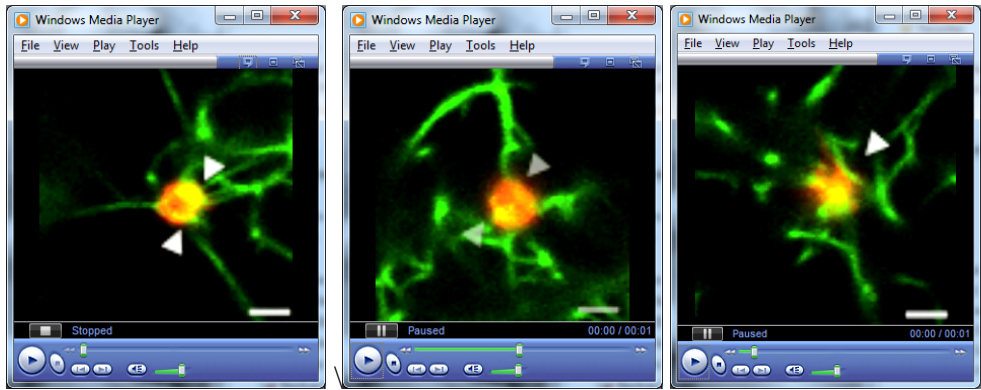
600 Figure 3: Biochemical and mechanical cues synergistically mediate platelet contraction force. **a**,  
601 Maximal platelet contraction occurs at 75kPa substrate stiffness and 1U/mL thrombin. **b**, Single  
602 platelet force quartiles for physiologically relevant clot stiffnesses and thrombin concentrations.  
603 Platelet contractile forces are highest at a substrate stiffness of 75 kPa or at 5U/mL thrombin. A  
604 minimum occurs at 25 kPa stiffness and 1U/mL thrombin. **c**, Exploded view of b to aid

605 visualization. Microenvironmental stiffness has a dominant role over thrombin concentration.  
606 Force attenuation at the highest stiffness conditions suggests a mechanically mediated negative  
607 feedback mechanism governing the upper limits of platelet contraction. n refers to total number  
608 of platelets tested.

609 Figure 4: Mechanotransductive platelet contraction is mediated by the Rho-associated protein  
610 kinase (ROCK) pathway, **as measured with platelet contraction cytometry and standard bulk clot**  
611 **contraction and bulk clot rheometry. a,** The increase in platelet contractile forces with increasing  
612 substrate stiffness is significantly reduced with exposure to Y27623, a pharmacologic ROCK  
613 inhibitor. Pharmacologic inhibition of the myosin light chain kinase (MLCK) with ML7, on the  
614 other hand, did not produce a statistically significant difference in the substrate stiffness-  
615 mediated effect on platelet contractile force. Box denotes median and quartiles; whiskers to 1.5  
616 interquartile range), square denotes median, triangles denotes 1% and 99%. (n = 539, each  
617 condition n>40). \* indicates differences from control at same stiffness (p < 0.05 by Mann-  
618 Whitney). **b, ROCK inhibition impairs bulk clot contraction (n = 4) as compared to the untreated**  
619 **control clots. c, MLCK inhibition does not change bulk clot contraction (n = 4). d,** Oscillatory  
620 **rheometry, which enables simultaneous measurements of storage and loss moduli as well as bulk**  
621 **tensile forces, revealed that both control and ROCK-inhibited clots undergo a dramatic stiffening**  
622 **process (representative plot from 3 similar experiments shown). The angular frequency and**  
623 **strain amplitude are 1 rad/s and 0.01, respectively, which are well within the linear regime of the**  
624 **samples. e, Control and ROCK-inhibited clots apply similar forces during the beginning of clot**  
625 **formation when the measured storage and loss moduli are low (n = 3). As the clots stiffen**  
626 **(Figure 4d), ROCK-inhibited bulk clots begin to exert lower tensile forces and plateau while the**  
627 **control continues to increase over time. \*\* indicates difference from control (p < 0.05 by t-test).**

628 Figure 5: Patients with phenotypic bleeding lack highly contractile platelets associated with clot  
629 contraction and force generation. **a**, Wiskott Aldrich Syndrome and May Hegglin Disorder  
630 platelets exhibited significantly reduced contractile forces compared to that of healthy controls  
631 (75 kPa gel stiffness, 1U/mL thrombin). In a subset of patients with bleeding diatheses yet  
632 normal hemostasis tests, platelet contraction was lower than that of normal healthy controls.  
633 **b**, Histogram data reveal platelet subpopulations of varying contractile forces. Healthy control  
634 platelets comprise high contractility subpopulations, notably absent in platelets from a Wiskott  
635 Aldrich Syndrome patient. In all panels, n refers to number of platelets, Mann-Whitney statistical  
636 test.

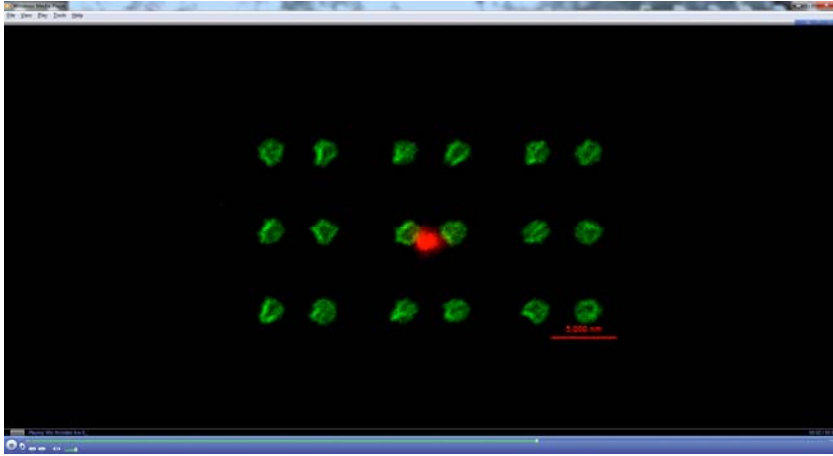
637 **Extended Data Videos**



638

639 Extended Data Video 1-3: Platelet contraction in 3d fibrin meshes span and pull adjacent fibers  
640 together of differing stiffness. The fibrin mesh has varying mechanical stiffness due to the  
641 differing thickness and cross linking point density. Here we show three platelets spanning fibrin  
642 filaments and pulling them together over the course of six minutes. White arrows point to same  
643 feature at both time points. Scale bar is 2  $\mu\text{m}$ .

644

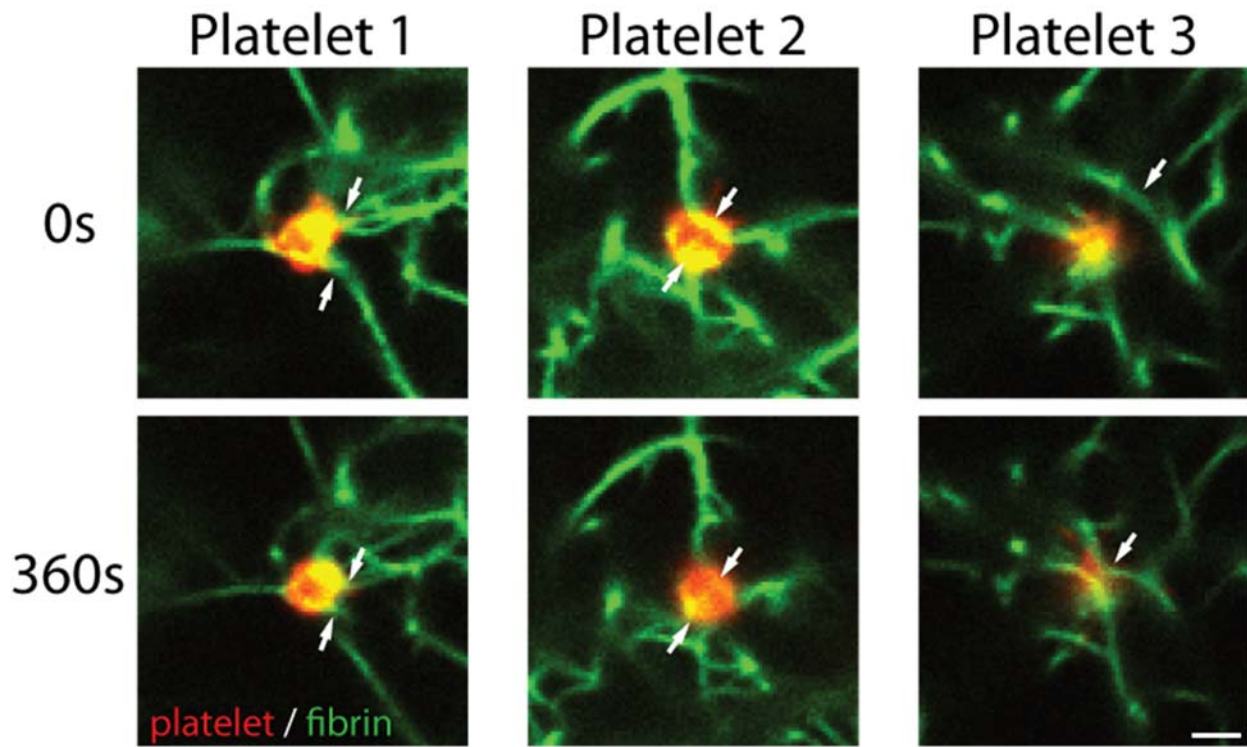


645

646 Extended Data Video 4: Individual contracting platelet - A single contracting platelet is imaged

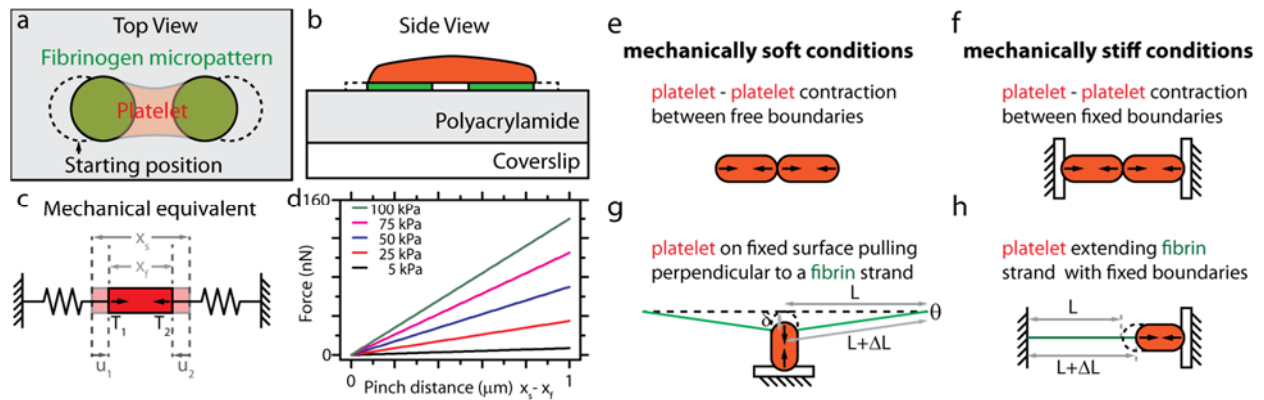
647 during the contraction process. Time elapsed for entire video is 60 minutes.

649



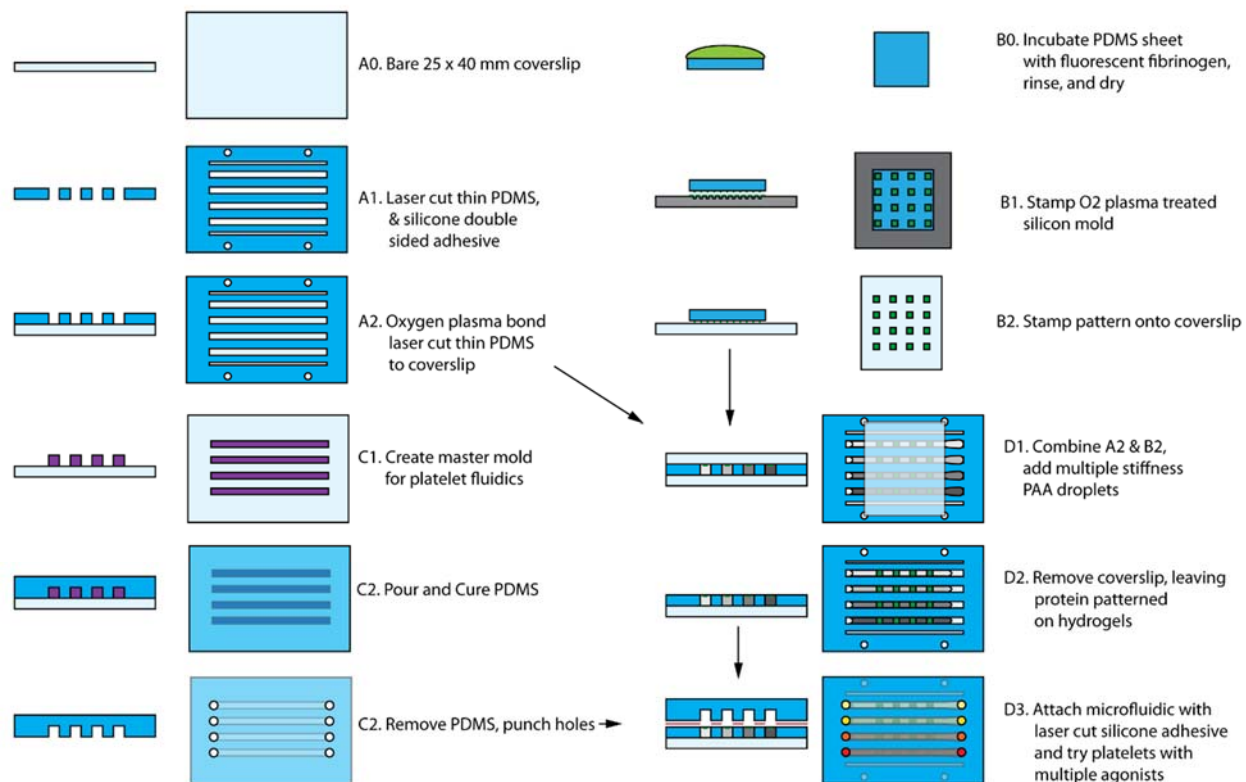
650

651 Extended Data Figure 1: Platelet contraction in 3d fibrin meshes span and pull adjacent fibers  
652 together of differing stiffness. The fibrin mesh has varying mechanical stiffness due to the  
653 differing thickness and cross linking point density. Here we show three platelets spanning fibrin  
654 filaments and pulling them together over the course of six minutes. White arrows point to same  
655 feature at both time points. Scale bar is 2  $\mu\text{m}$ .



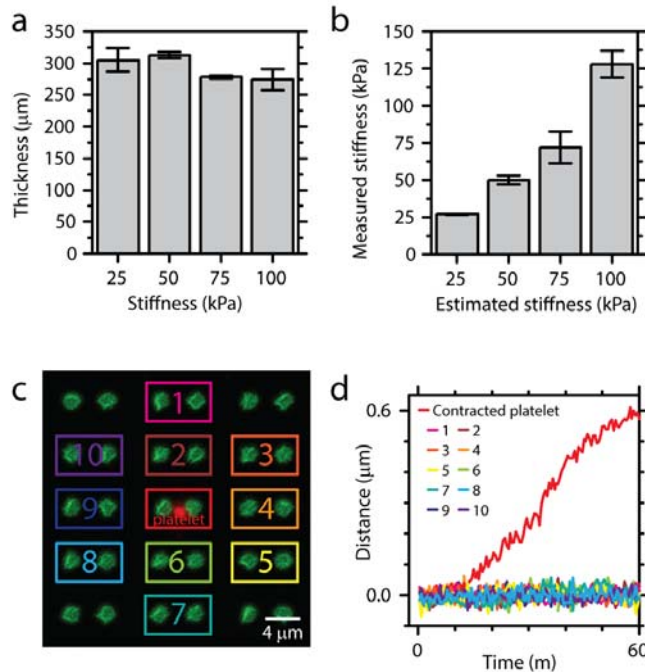
656

657 Extended Data Figure 2: Contractile system, mechanical model, and calculated forces as a  
 658 function of pinch distance, and limiting cases for stiffness. **a-b**, The fibrinogen patches are  
 659 covalently attached to the underlying hydrogel and move independently. **c**, Mechanically, this  
 660 can be modeled as a platelet pulling on two springs of equivalent stiffness. **d**, The force a platelet  
 661 will exert by pulling the fibrinogen patches together may be calculated from a measurement of  
 662 the pinch distance for a range of different hydrogel stiffnesses. When considering force range, it  
 663 is important to consider the limiting cases defining mechanical stiffness values **e**, Platelets  
 664 contracting against one another with moving boundaries are expected to have stiffness on the  
 665 order of 10 kPa, the value for an activated contracted platelet. **f**, Platelets contracting in between  
 666 fixed boundaries experience isometric contraction. Previous measurements in isometric  
 667 contractile conditions found maximal forces of 80nN. **g**, Platelets pulling a fibrin strand  
 668 perpendicular to the principle axis will cause minimal extension of the fibrin, exerting single  
 669 nanonewton forces. **h**, Platelets which extend a single fibrin fiber will need to exert several 10s  
 670 of nanonewtons. Neither g nor h consider pre-strain in the fibrin or multiple fibers which will  
 671 make the conditions much stiffer.



672

673 Extended Data Figure 3: Detailed process flow for construction of microfluidic traction force  
 674 microscopy test device. Due to the commercial availability of most starting materials, batches of  
 675 devices may be made in less than 8 hours.



676

677 Extended Data Figure 4: Cast polyacrylamide gels in laser cut gaskets are equivalent to macro

678 systems and enable independent measurements of platelet contractile forces. **a**, Measurements of

679 polyacrylamide gels in channels demonstrate that gels are thicker than 70 μm to ensure that the

680 underlying glass substrate does not contribute to the locally measured stiffness (n = 4, error bars

681 show standard deviation). **b**, The measured stiffness values are in agreement with estimated

682 values, and similar to previously published values in the literature. (n = 18 from two different

683 gels, error bars show standard deviation) **c-d**, A single contracting platelet on a microdot pair

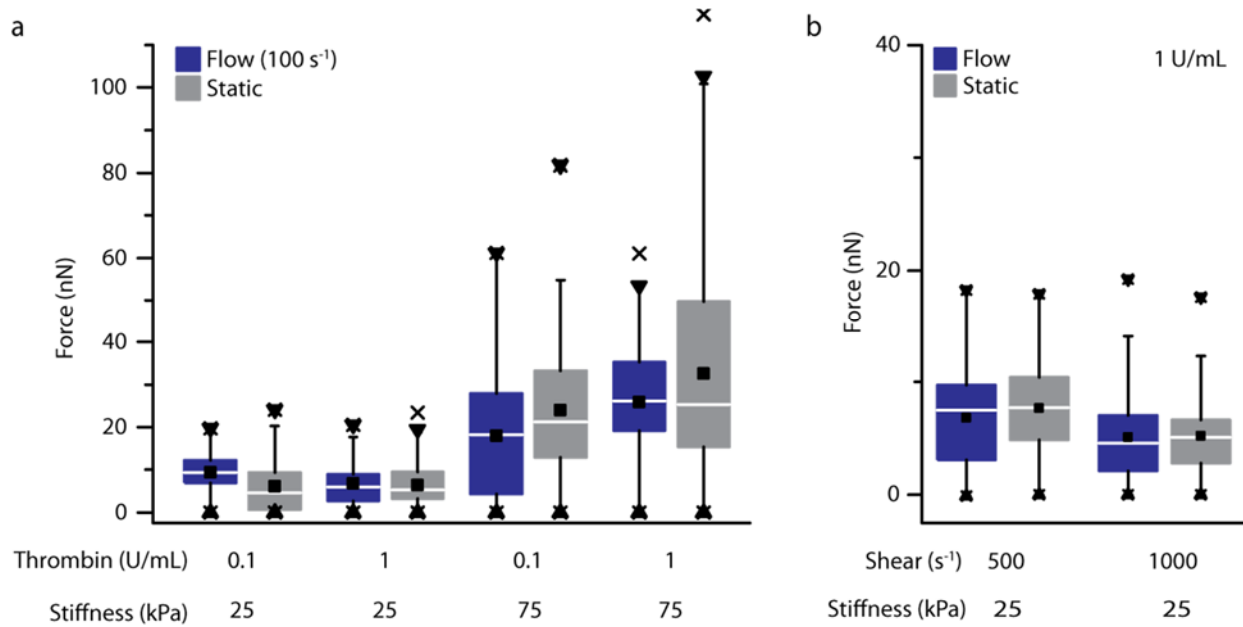
684 does not affect the displacement of the surrounding microdot pairs, demonstrating that each

685 microdot pair is independent from the neighbor.

686

687

688



689

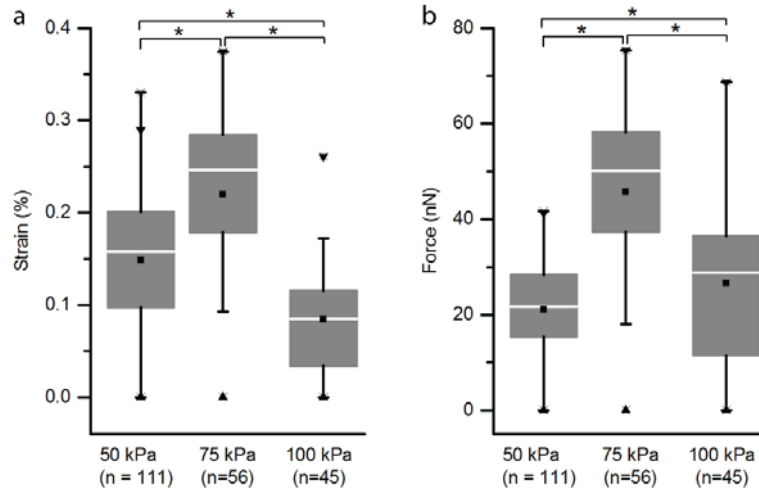
690

691

692

693

Extended Data Figure 5: Application of shear stress after the initiation of adhesion and contraction has no statistical change on platelet contractile forces. (a) Shear flow was applied at 100 s<sup>-1</sup> with differing stiffness and thrombin concentration (b) Differing shear was applied at 25 kPa and 1 U/mL thrombin. ( $n_{\text{condition}} \geq 35$ ,  $n_{\text{total}} = 887$ )



694

695

696

697

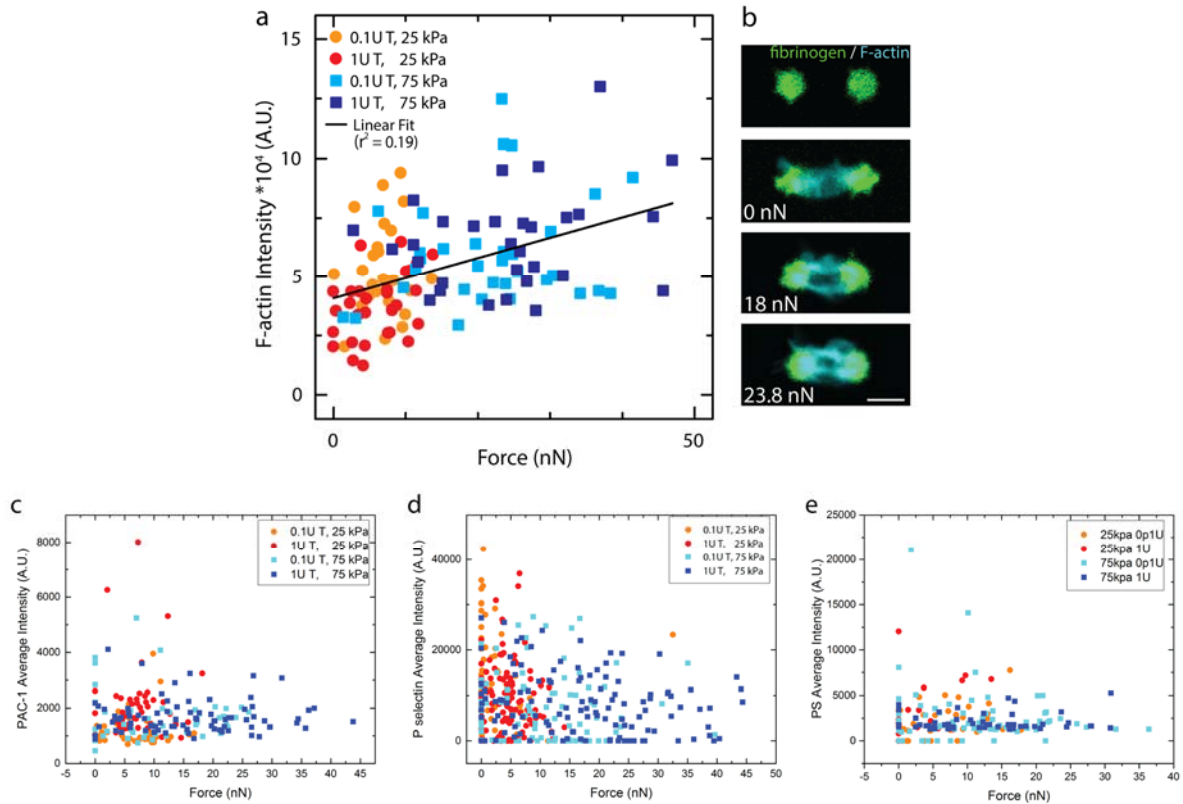
698

699

700

701

Extended Data Figure 6: Platelet microdot displacement and force is reduced as the environmental stiffness increases. **a**, Measured microdot displacements become small when the environmental stiffness is very high at 100 kPa. **b**, When converted to force, the distances measured in (a) reveal that a similar range of forces is seen between 75 kPa and 100 kPa stiffness gels, but that the average force is lower, indicating that on average platelets do not apply high contraction forces efficiently in very high stiffness environments. Significance by Mann-Whitney,  $\alpha < 0.05$ .



703

704 Extended Data Figure 7: F-actin intensity weakly correlates with platelet contractile force, and

705 no discernible correlation is seen with other markers of platelet activation. **a**, F-actin content

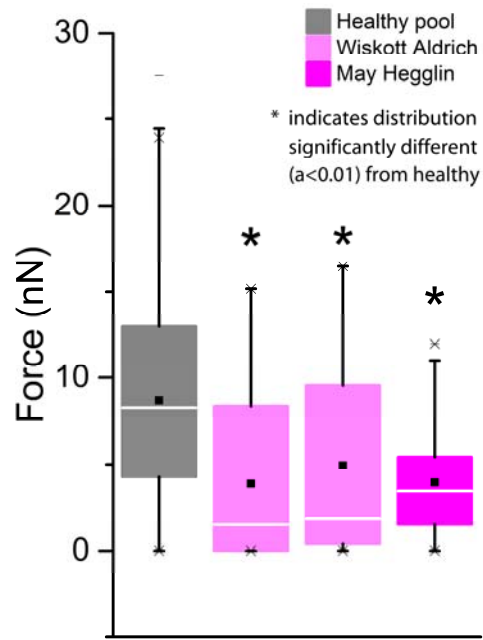
706 weakly correlates with contractile force in a variety of different thrombin and mechanical

707 conditions. Correlation of  $r > 0.3$  at  $\alpha = 0.05$ . **b**, Selected images of a separate experiment with

708 0.1 U/mL thrombin and 25 kPa of some platelets showing increase and improved organization in

709 F-actin with increasing contractile force. As indicated in **a**, there were also some platelets which710 did not follow this trend. Little to no correlation in force and **c**, PAC-1 binding, **d**, P-selectin711 binding, or **e**, PS exposure was observed.

712

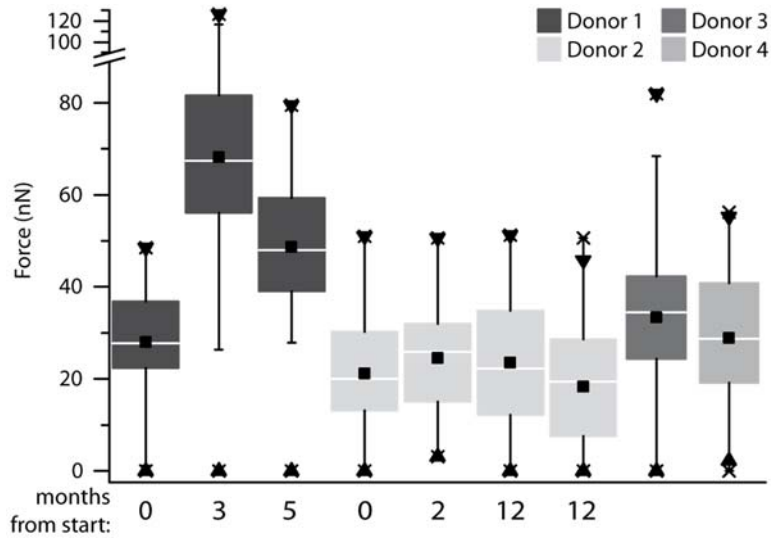


713

714 Extended Data Figure 8: Platelet contractile forces are impaired in individuals with acto-myosin

715 related cytoskeletal mutations on soft gels. ( $n_{\text{patient}} \geq 28$ ,  $n_{\text{total}} = 598$ )

716  
717  
718



719  
720

721 Extended Data Figure 9: Platelet contraction for the same donor over time with numbers  
722 indicating time from start. Donor 1 and donor 2 defined the limits of the contraction range  
723 measured for healthy individuals, with donor 1 having a high variability in between  
724 measurements and donor 2 having exceptionally low variability in between measurements.  
725 Donors 3 and 4 were measured at a later time point in the study. ( $n_{\text{patient}} \geq 30$ ,  $n_{\text{total}} = 616$ )

726

727

Study ID	Contractile force	Bleeding history	Plt count (10 <sup>3</sup> /uL)	PT (s)	aPTT (s)	fibrinogen (mg/dL)	Factor VIII assay (%)	VWF Ag (%)	Ristocetin cofactor	thrombin time (s)
WL05		easy bruising, spontaneous hematomas, hematuria, occasional nosebleeds	210	13.5	30.6	307	137	107	107	16.8
WL02		heavy menstruation, easy bruising and gum bleeding	229	14	28.9	255	134	96	62	14.9
WL06	low	frequent prolonged nosebleeds, gum bleeding	245	14.6	29.5	330	127	79	78	16.4
WL07	low	frequent nosebleeds	348	14.3	29.2	227	163	165	81	19.3
WL03	very low	heavy menstruation, easy bruising, frequent gum bleeding and nosebleeds	240	13.3	29.9	343	183	60	54	16.4

728

729 Extended Data Table 1: Patient history and labs for individuals with unknown bleeding disorders

730

731

732

Study ID	Contractile force	Platelet aggregation interpretation by hematopathologist	PFA
WL05		normal platelet aggregation and release with ADP, arachadonic acid, collagen, ristocetin (low and high dose), thrombin	closure time with collagen/epi - 106 s (normal:83-163 s) and collagen/ADP - 73 s (normal:72-111 s)
WL02		normal platelet aggregation and release with ADP, arachadonic acid, collagen, ristocetin (low and high dose), thrombin	closure time with collagen/epi - 243 s (normal:83-163 s) and collagen/ADP - 174 s (normal:72-111 s) but Hct at 19.4
WL06	low	normal platelet aggregation and release with ADP, arachadonic acid, collagen, ristocetin (low and high dose), thrombin	closure time with collagen/epi - 116 s (normal:83-163 s) and collagen/ADP - not reported (normal:72-111 s)
WL07	low	Mildly decreased aggregation to low and high dose collagen, with normal ATP release. Given all other agonists are normal, this finding likely is clinically insignificant. Repeat testing may be performed if clinically indicated	closure time with collagen/epi - 107 s (normal:83-163 s) and collagen/ADP - 68 (normal:72-111 s)
WL03	very low	normal platelet aggregation and release with ADP, arachadonic acid, collagen, ristocetin (low and high dose), thrombin	closure time minimally elevated with collagen/epi - 177 s (normal:83-163 s) and collagen/ADP - 116 s (normal:72-111 s)

733

734 **Extended Data Table 2: Interpretation of history and labs for individuals with unknown bleeding disorders by hemopathologist with**

735 **PFA data**

736

## **Device design: Mechanics**

### **Surface traction force microscopy**

By constraining lithographically patterned arrays of fluorescently tagged proteins to a polyacrylamide gel surface, the computational and experimental constraints of traditional traction force microscopy are greatly reduced<sup>29</sup>. As cells adhere and move protein microdots, the independent traction force,  $\mathbf{T}$ , is calculated as:

$$\mathbf{T} = \frac{2\pi G a \mathbf{u}}{2 - \nu}$$

where  $G$  is the shear modulus,  $a$  is the microdot radius,  $\nu$  is Poisson's ratio, and  $\mathbf{u}$  is the displacement vector. By measuring the displacement of the microdot relative to the starting position, the applied force is calculated. Since the shear modulus of polyacrylamide gels may be changed by changing the ratios of precursor materials<sup>33</sup>, the mechanical stiffness felt by the platelet may be changed independent of other parameters such as the ligand area and density.

### **Simplification of traction force microscopy with two microdot system**

Noting that in fibrin clots, platelets may span and pull together two surfaces (Extended Data Figure 1), the method above may be simplified even further by spatially separating microdots such that platelets preferentially attach to two microdots (Extended Data Figure 2a-b). Here, since the gel stiffness is constant, each microdot may be treated as a spring of equivalent stiffness,  $k$ , displaced from an equilibrium position  $u_1$  or  $u_2$ , as long as the microdot areas are approximately equal (Extended Data Figure 2c). By static equilibrium,  $u_1 = u_2$ , and the displacement of each microdot is:

$$u_1 = u_2 = \frac{1}{2}(x_s - x_f)$$

where  $x_s$  is the starting distance of the microdots, and  $x_f$  is the final distance of the microdots.

The traction force applied by the platelet is the sum of the applied traction forces and may be rewritten in terms of starting distance and final distance.

$$T = T_1 + T_2 = \frac{2\pi Ga u_1}{2 - \nu} + \frac{2\pi Ga u_2}{2 - \nu} = \frac{2\pi Ga}{2 - \nu}(x_s - x_f)$$

By rewriting the equations in this form, image post-processing is greatly simplified as only two measurements are needed: the final contracted distance and the original uncontracted distance.

Using this equation, the force as a function of pinch distance may be calculated for a variety of different gel stiffnesses (Extended Data Figure 2d). Due to the high precision lithography used here, the uncontracted distance may be assumed to be the distance of a neighboring unperturbed pair of microdots, and all measurements are performed once the experiment is completed.

### **Ligand size choice and spacing**

Using a micropatterning<sup>29</sup> approach to traction force microscopy, both ligand area, ligand density, and system stiffness could be independently controlled and tuned to mimic geometries and mechanical stiffnesses experienced in clots. In consideration of the platelet size and mindful of lithography and fabrication minimum feature size constraints, we created pairs of fibrinogen circular microdots with a radius of 0.8  $\mu\text{m}$ , and center to center distance of 4  $\mu\text{m}$  (Figure 1).

These numbers are similar to those seen in previous AFM studies showing that platelets spread to an area of approximately 1  $\mu\text{m}^2$  when pulling together two fibrinogen coated surfaces<sup>8</sup>, with

microdot displacements of approximately  $0.5 - 1 \mu\text{m}$ . Such numbers also appeared to be in agreement with our own images of platelets contracting in fibrin gels (Extended Data Figure 1, Extended Data Video 1). By spacing pairs of microdots least  $8 \mu\text{m}$  apart<sup>8</sup>, platelet contraction was effectively confined to a single pair of microdots (Figure 1b)<sup>9</sup>.

The size of the microdots was an important parameter in confining the platelet interaction to two microdots. Platelets are less likely to span to a neighboring microdot when the microdot is large, whereas platelets may span many microdots if the microdots are small and closer together. Aside from creating an appropriate spatial geometry to interact with platelets, the microdot size is also appropriate for optical microscopy. Similarly, based on our force calculations, the microdot size is of an appropriate size to confer adequate force sensitivity and resolution. It is important to note that since the microdot is also a signaling molecule for platelet contraction via  $\alpha_{\text{IIb}}\beta_3$ , that changes in the size could affect platelet behavior. However, any changes in platelet behavior due to a limited ligand area will be systemic since the ligand area is constant for all experiments. Moreover, the data is in agreement with previous atomic force microscopy studies<sup>8</sup>, which did not constrain ligand area. Also, since the ligand area also matches *in vitro* clot observations, any errors are expected to be minimal.

After establishing a system of appropriate spatial dimensions, we sought to ensure that the stiffness encountered by platelets was similar to those found in clots. At the single platelet level, this system is expected to be an analog for either platelet-platelet interactions or platelet-fibrin interactions, which are the primary interactions within a clot. A large variety of mechanical stiffnesses are encountered within clots, which have bulk elastic moduli between  $45 - 70 \text{ Pa}$ <sup>36</sup>. Activated contracted platelets have stiffness values of  $\sim 10 \text{ kPa}$ <sup>7</sup>; whereas individual fibrin fibers

have stiffness values of 2 MPa (unligated) or 14.5 MPa (ligated)<sup>37</sup>. Using such values it is possible to factor local geometric considerations to estimate the mechanical stiffness and forces that platelets are likely to encounter within a clot. Here the goal is to choose an appropriate range of PAA gel stiffnesses for use within our system. As such, these estimates will focus on limiting cases for the mechanical environment surrounding platelets. This analysis could be carried forth from many different perspectives, but here, expected forces on platelets will be calculated and compared to values achievable with this system (Extended Data Figure 2c)

For platelet-platelet interactions, two limiting cases are considered: when contracting platelets have free boundaries (Extended Data Figure 2e) and when contracting platelets have fixed boundaries (Extended Data Figure 2f). The free boundary case represents the softest interaction which could be experienced by platelet-platelet interactions. In the simplified case, platelets are free to contract and will apply no force to do so. Practically, the material properties of individual platelets will play a dominant role in defining the stiffness of the system. Previous AFM studies have determined that activated, contracted platelets have stiffness of 10 kPa<sup>8</sup>. Hence, forces associated with such systems are expected to be low on the order of several nN. The fixed boundary case represents an interaction in an infinite stiffness environment, where platelets experience isometric contraction. Previous studies have already studied such cases and determined that contractile forces tend to maximum around 80 nN<sup>8</sup>. Our fibrinogen microdots must move in order for contraction to be measured, so PAA gel stiffnesses were chosen which would enable platelets to achieve similar forces with less than 1  $\mu\text{m}$  of contraction. Here, both 75 kPa and 100 kPa gel stiffness meet this criteria (Extended Data Figure 2d).

For platelet-fibrin interactions, the limiting cases are defined by the direction in which a platelet pulls on a single fibrin strand, either perpendicular (Extended Data Figure 2g) or parallel

(Extended Data Figure 2h). Using atomic force microscopy and fibrin fibers spanned across gaps, others have demonstrated that tension built in fibrin networks is through extension of the fibrin and not applied moments. Using published values<sup>37</sup> for typical ligated fibrin diameters ( $284 \pm 44$  nm), lengths ( $14.7 \pm 2.5$   $\mu$ m), and modulus ( $14.5 \pm 3.5$  MPa), the forces associated with these two conditions may be estimated.

When the platelet pulls perpendicular to the fibrin strand the extension is minimal representing the limit of the soft mechanical environment. Here, assuming a 0.5  $\mu$ m platelet contraction, the strain,  $\epsilon$ , is then:

$$\epsilon = \frac{\Delta L}{L} = \frac{\sqrt{\delta^2 + L^2} - L}{20} = \frac{\sqrt{0.5^2 + 7.35^2} - 7.35}{7.35} = 0.0023$$

The associated angle is then:

$$\theta = \tan^{-1}\left(\frac{0.5}{7.35}\right) = 0.07$$

Due to symmetry in this system, and in consideration of static equilibrium, the force applied by the fibrin to the platelet is then:

$$F \sin \theta = E A \epsilon \sin \theta = (14.5 \text{ MPa}) \left(\frac{\pi}{4} (284 \text{ nm})^2\right) (0.0023) (\sin 0.07) = 0.15 \text{ nN}$$

When the platelet pulls the parallel to the fibrin strand, the extension is maximized. Assuming that the platelet is capable of pulling 0.5  $\mu$ m, the associated strain is then:

$$\epsilon = \frac{\Delta L}{L} = \frac{0.5}{14.7} = 0.034$$

The force is then

$$F = E A \epsilon = (14.5 \text{ MPa}) \left( \frac{\pi}{4} (284 \text{ nm})^2 \right) (0.034) = 31 \text{ nN}$$

Also, if a platelet were pulling on unligated fibers in the developing clot (pre Factor XIII), then these values would be an order of magnitude lower. Hence, in examining these limiting cases and previously published values for platelet contraction, choosing PAA gels of stiffness between 5 and 100 kPa (Extended Data Figure 2d) will adequately cover the micromechanical stiffness environment that a platelet will experience within a typical clot.